Electronic Supplementary Information

Novel organo-osmium(II) proteosynthesis inhibitors active against human ovarian cancer cells reduces gonad tumor growth in *Caenorhabditis elegans*

Enrique Ortega,[a,+] Francisco J. Ballester,[a,+] Alba Hernández-García,[a] Samanta Hernández-García,[b] M. Alejandra Guerrero-Rubio,[b] Delia Bautista,[c] M. Dolores Santana[a,*] Fernando Gandía-Herrero,[b,*] and José Ruiz [a,*]

[a.] *Departamento de Química Inorgánica, Universidad de Murcia, and Institute for Bio-Health Research of Murcia (IMIB-Arrixaca), E-30071 Murcia, Spain.*

[b.] *Departamento de Bioquímica y Biología Molecular A, Unidad Docente de Biología, Facultad de Veterinaria, Universidad de Murcia, E-30071 Murcia, Spain.*

[c.] *SAI, Universidad de Murcia, E-30071 Murcia, Spain.*

Email: jruiz@um.es; fgandia@um.es; dsl@um.es.

[+] These authors contributed equally to this work.

Table of Contents

1. Instrumentation

The ^{1}H and ^{13}C NMR spectra were recorded on Bruker AC 300E and Bruker AV 400. Chemical shifts are cited relative to the residual ^{1}H and ^{13}C solvent peaks. The complexes were analyzed via multinuclear 2D (^{1}H-^{1}H COSY and ^{1}H-^{13}C HSQC) NMR spectroscopic experiments that allowed unambiguous assignments of all resonances. UV/vis spectroscopy was carried out on a PerkinElmer Lambda 750 S spectrometer with operating software. ESI mass (positive mode) analyses were performed on a HPLC/MS TOF 6220. The isotopic distribution of the heaviest set of peaks matched very closely that calculated for the formulation of the complex cation in every case. The FT-IR spectra were recorded on a Perkin-Elmer 1430 spectrophotometer using KBr disc. The C, H, N and S analyses were performed with a Carlo Erba model EA 1108 microanalyzer.

2. Reagent and solvents

All synthetic manipulations were carried out under an atmosphere of dry nitrogen using standard Schlenk techniques. Solvents were dried by the usual methods. Pyridine, 4-(dimethylamino)pyridine, 4-(2-piridyl)benzaldehyde, 2-phenylpyridine ligands, sodium acetate, dimethyl sulfoxide (DMSO), osmium(III) chloride hydrate and CDDP were obtained from Sigma-Aldrich (Madrid, Spain). $[(\eta^{6}\text{-}p\text{-cymene})OsCl_2]_2$ was prepared as previously reported. Deuterated solvents were obtained from Euriso-top.

For cellular studies, stock solutions were prepared by dissolving the compounds in DMSO to a final concentration of 20 mM and serially diluted prior to testing in DMSO. The final DMSO concentration in culture medium did not exceed 0.4 % (v/v) to avoid DMSO toxicity. CDDP stock solution was prepared by dissolving CDDP in ultrapure water (Milli-Q®, Merck Millipore) to a final concentration of 20 mM.

3. Schemes of synthesis

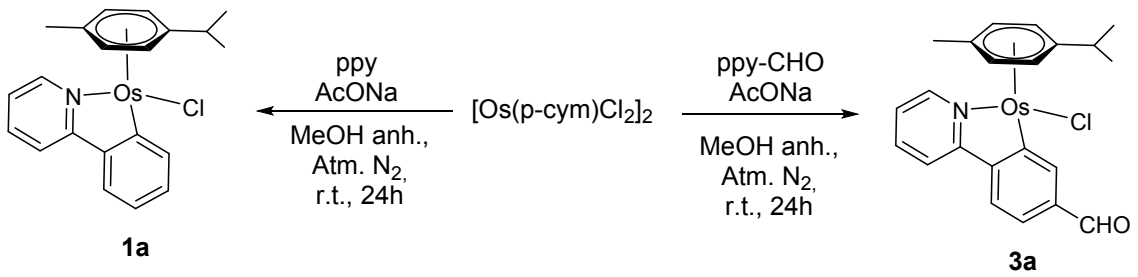

Scheme S1. Synthesis of complexes **1a** and **3a**.

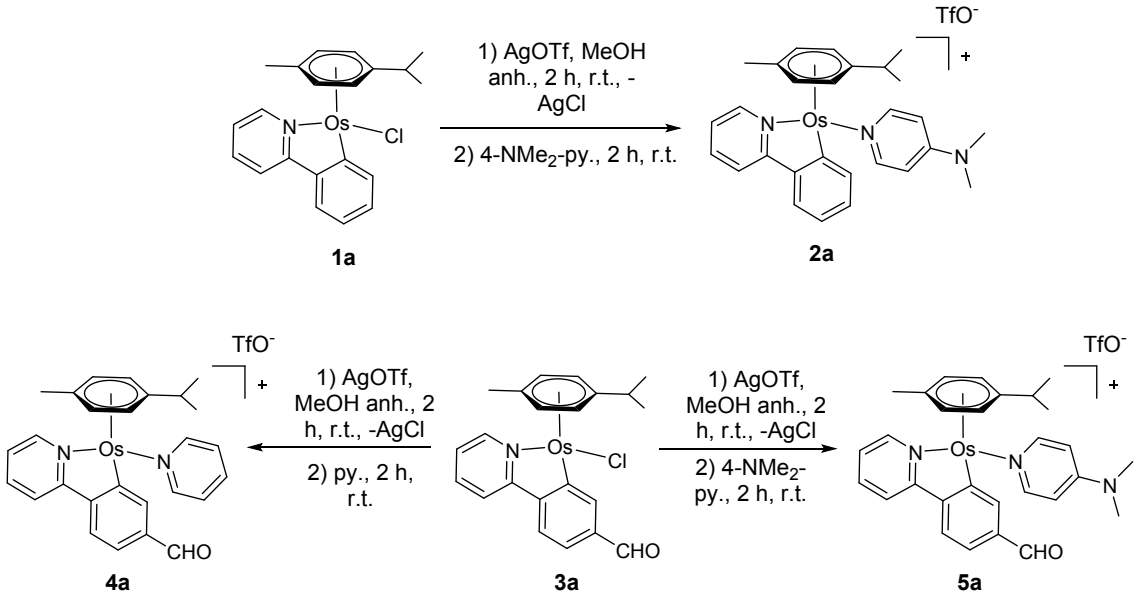

Scheme S2. Synthesis of complexes **2a, 4a** and **5a**.

4. NMR spectra of compounds 1a-5a

Compound 1a

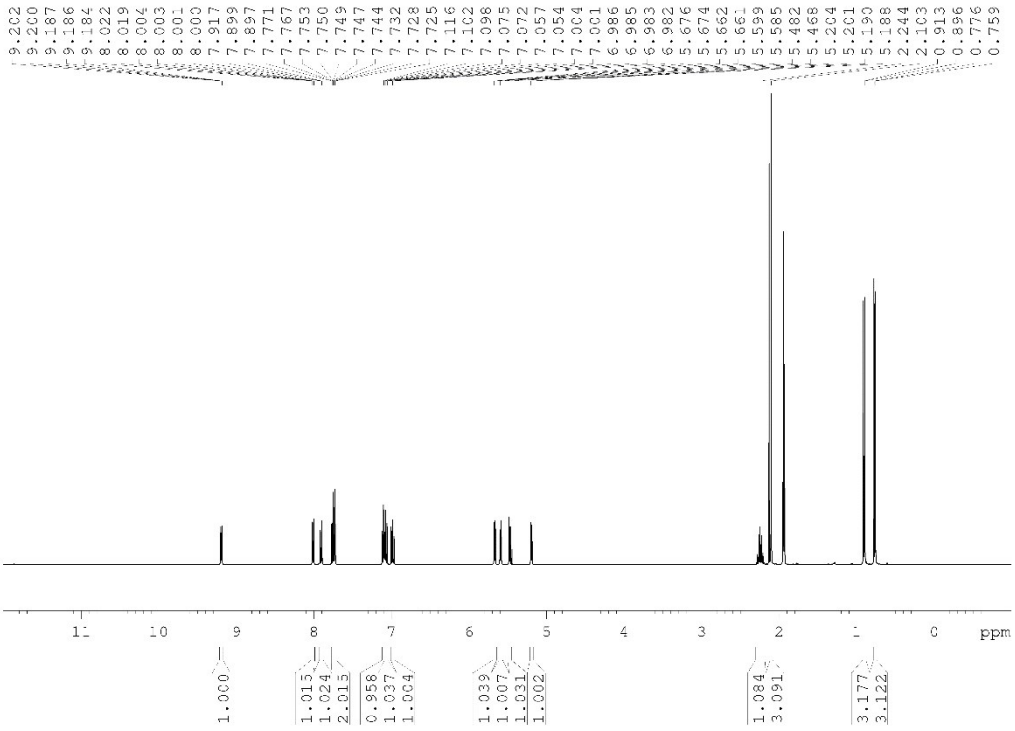

Figure S1. 400 MHz ^{1}H NMR spectrum of complex **1a** in CD_3CN.

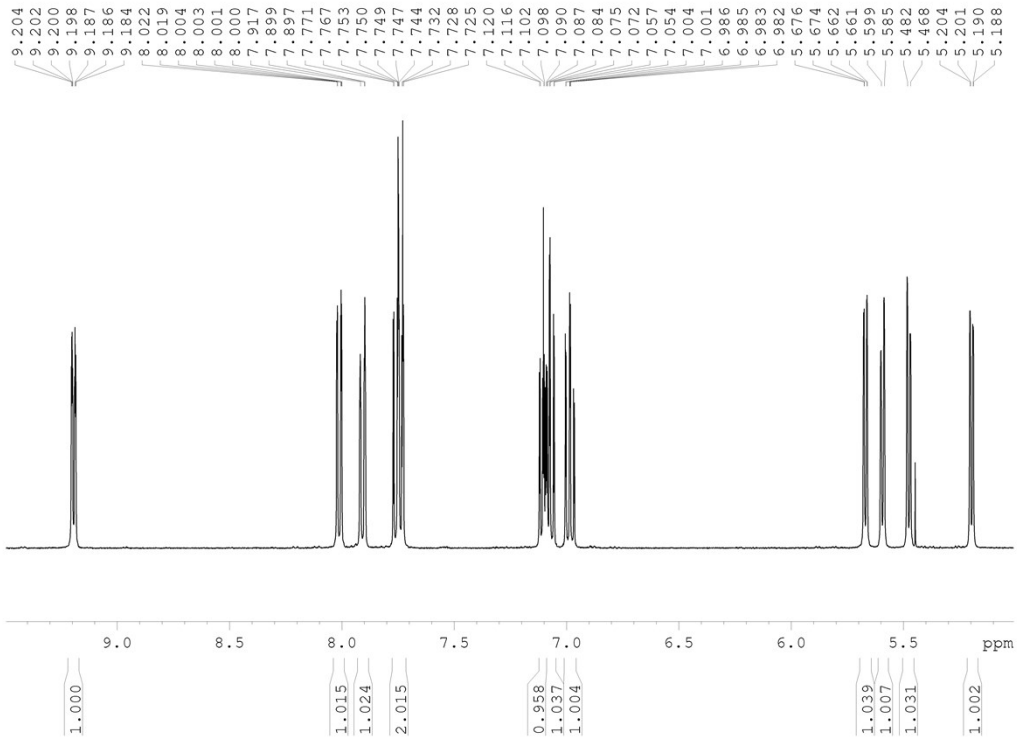

Figure S2. Aromatic region of ^{1}H NMR spectrum of complex **1a** in CD_3CN

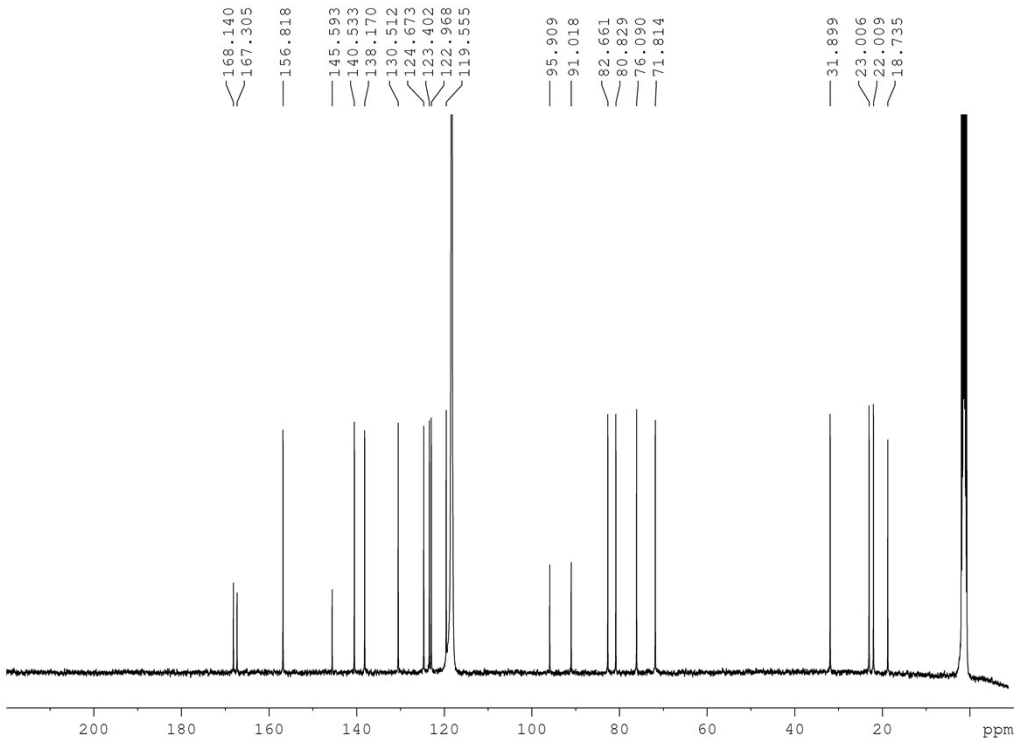

Figure S3. 101 MHz ^{13}C NMR spectrum of complex **1a** in CD_3CN

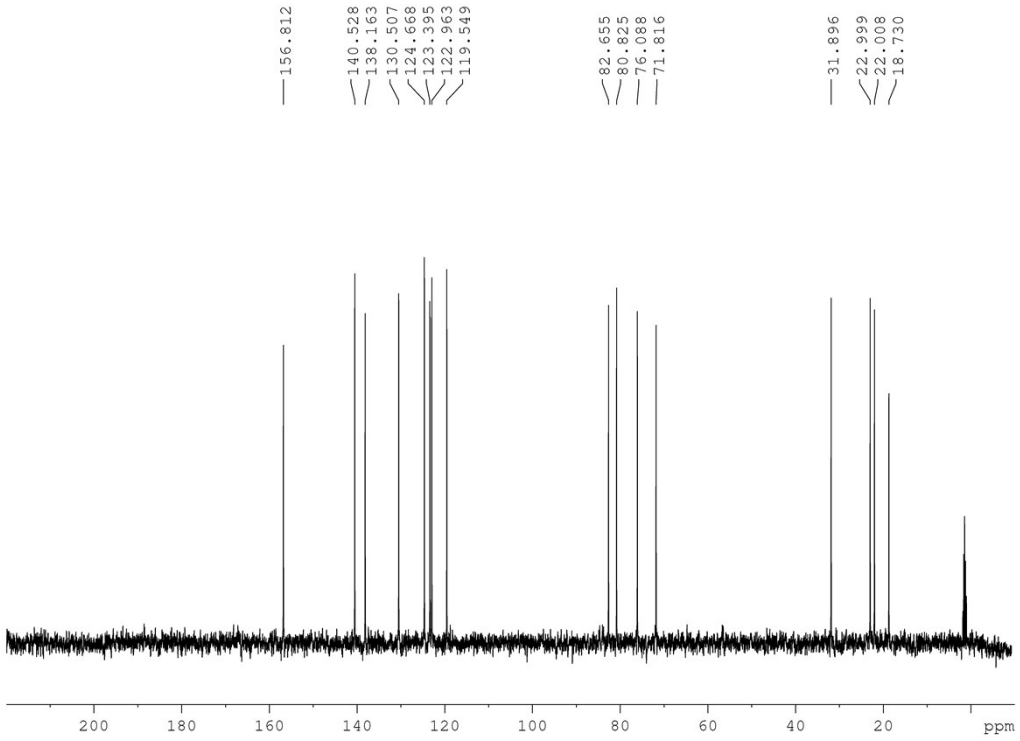

Figure S4. 101 MHz DEPT-135 NMR spectrum of complex **1a** in CD_3CN.

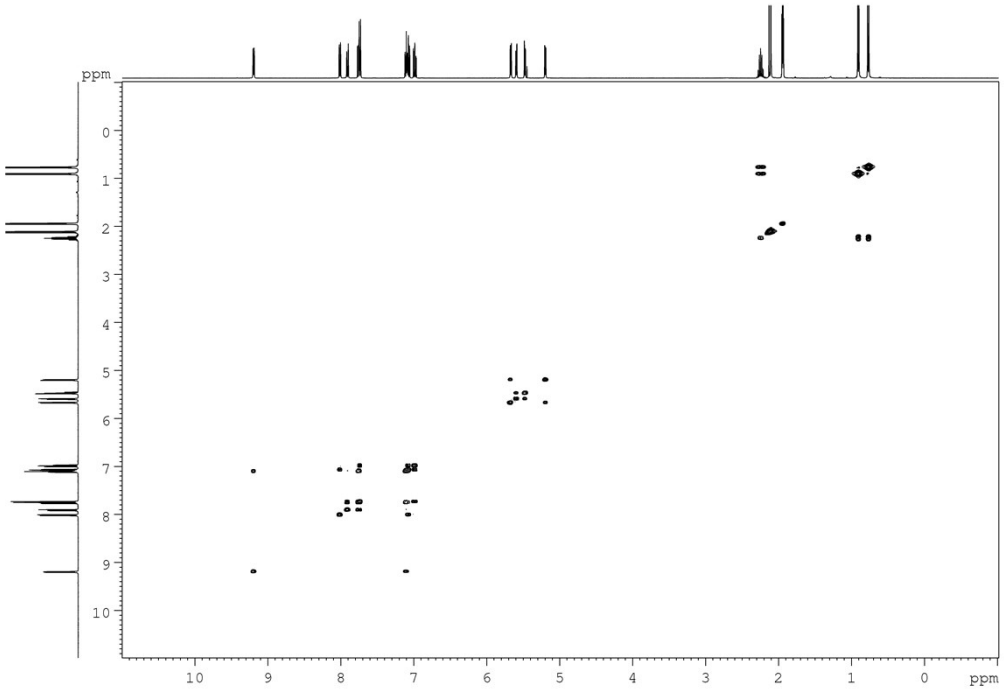

Figure S5. 400 MHz [^{1}H, ^{1}H]-COSY NMR spectrum of complex **1a** in CD_3CN

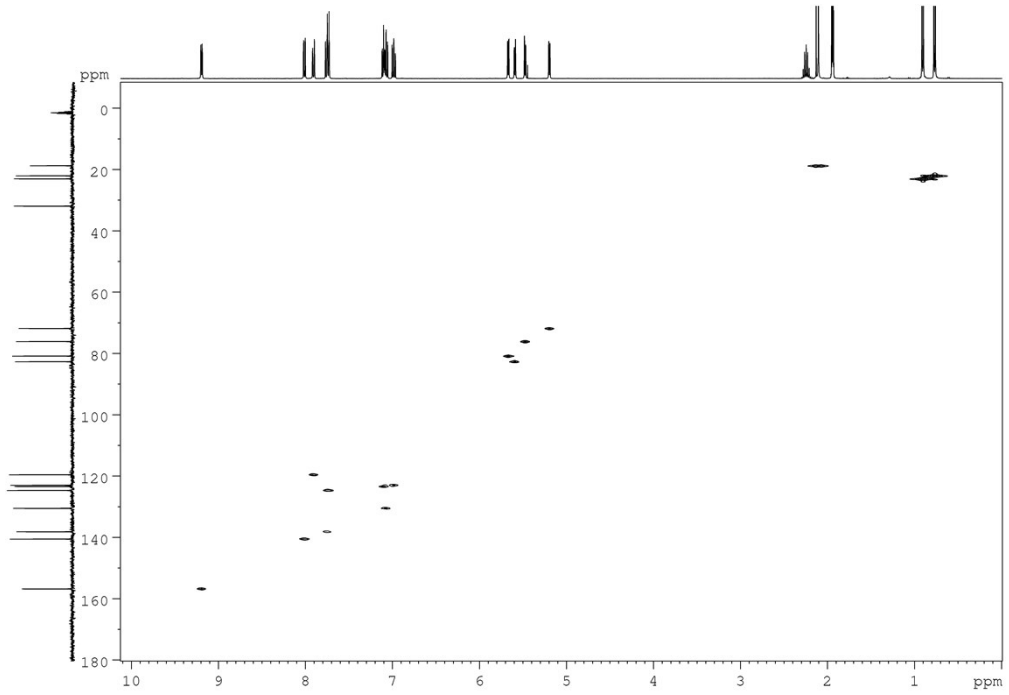

Figure S6. [^{1}H, ^{13}C]-HMQC 2D NMR (^{1}H, 400 MHz) spectrum of complex **1a** in CD_3CN

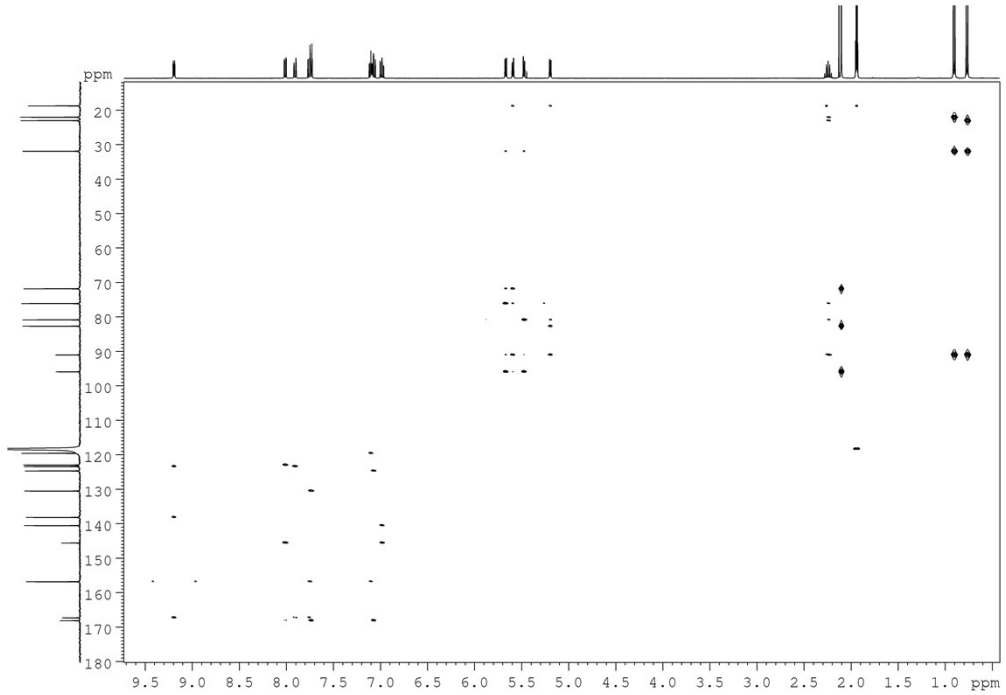

Figure S7. [^{1}H, ^{13}C]-HMBC 2D NMR (^{1}H, 400 MHz) spectrum of complex **1a** in CD_3CN

Compound 2a

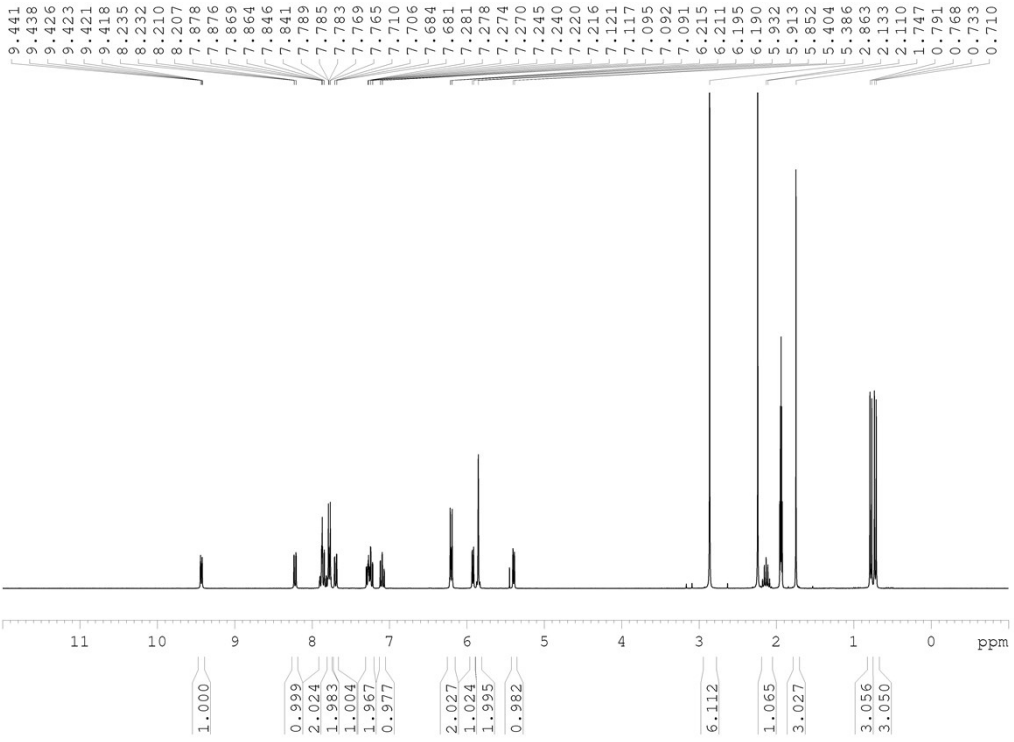

Figure S8. 300 MHz ^{1}H NMR spectrum of complex **2a** in CD_3CN

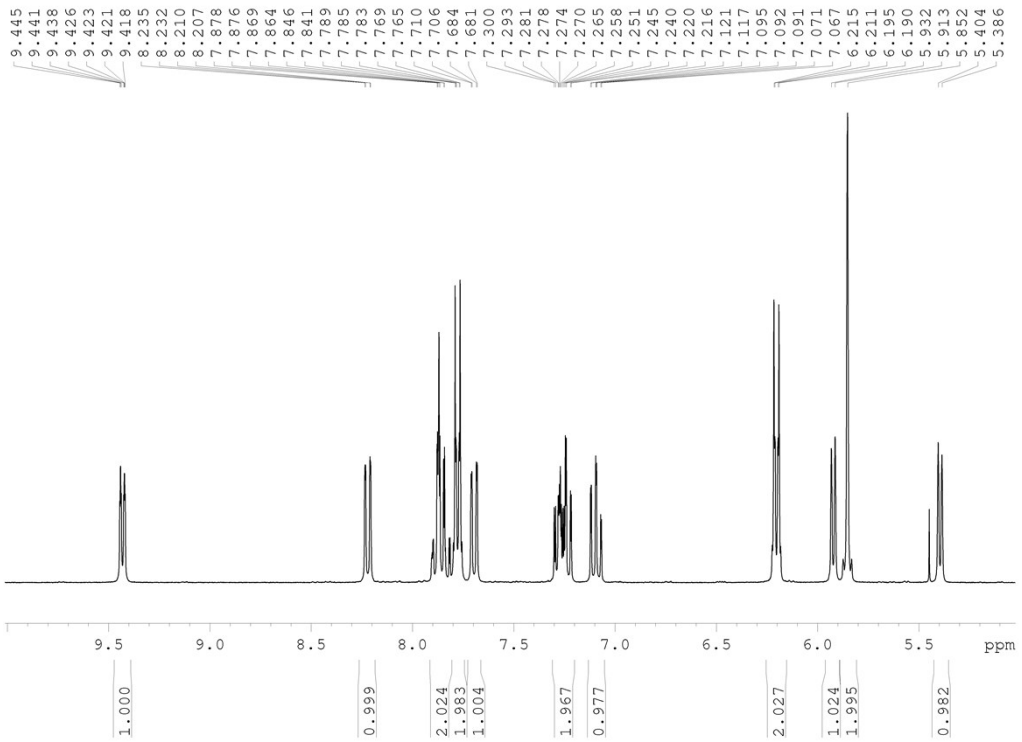

Figure S9. Aromatic region of ^{1}H NMR spectrum of complex **2a** in CD_3CN.

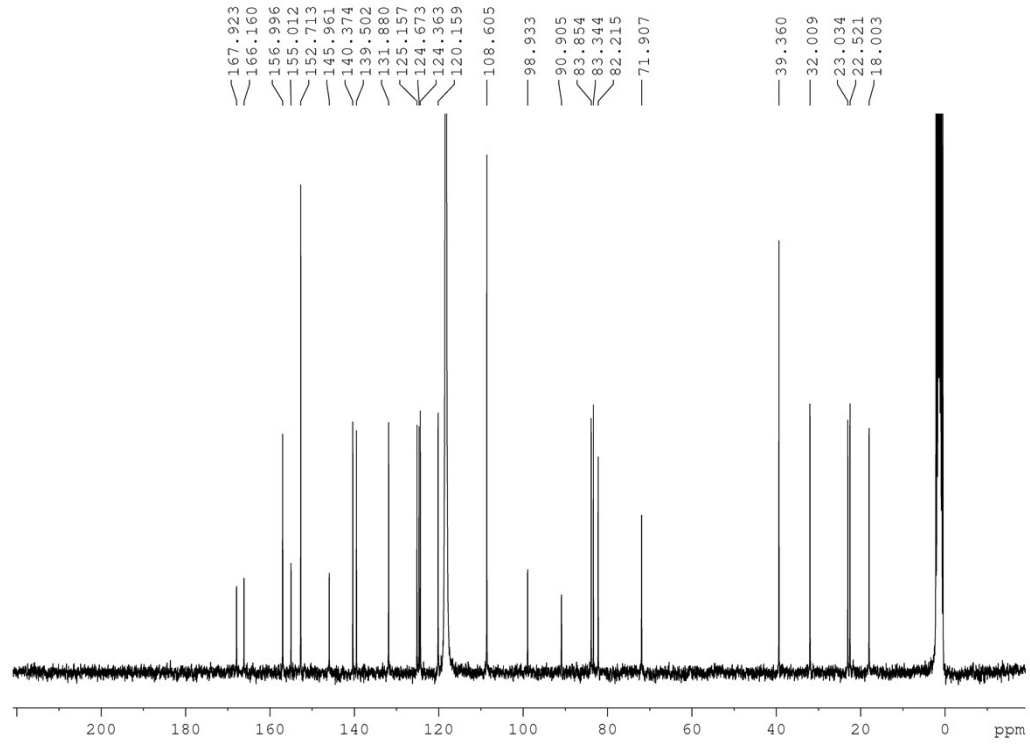

Figure S10. 75 MHz ^{13}C NMR spectrum of complex **2a** in CD_3CN.

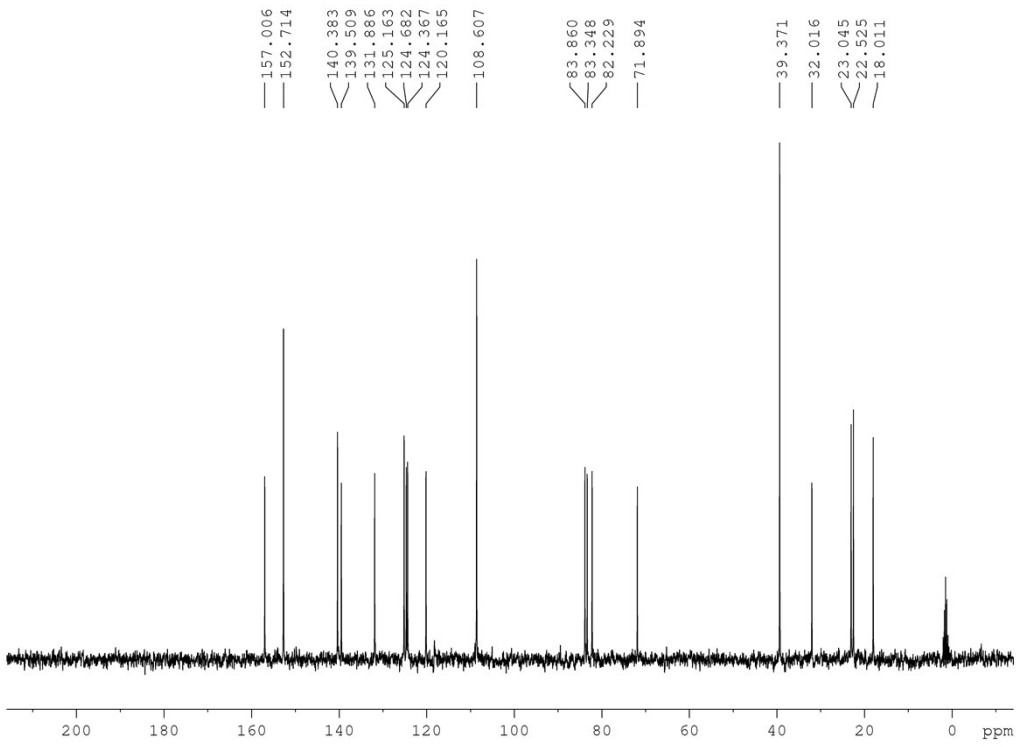

Figure S11. 75 MHz DEPT-135 NMR spectrum of complex **2a** in CD_3CN.

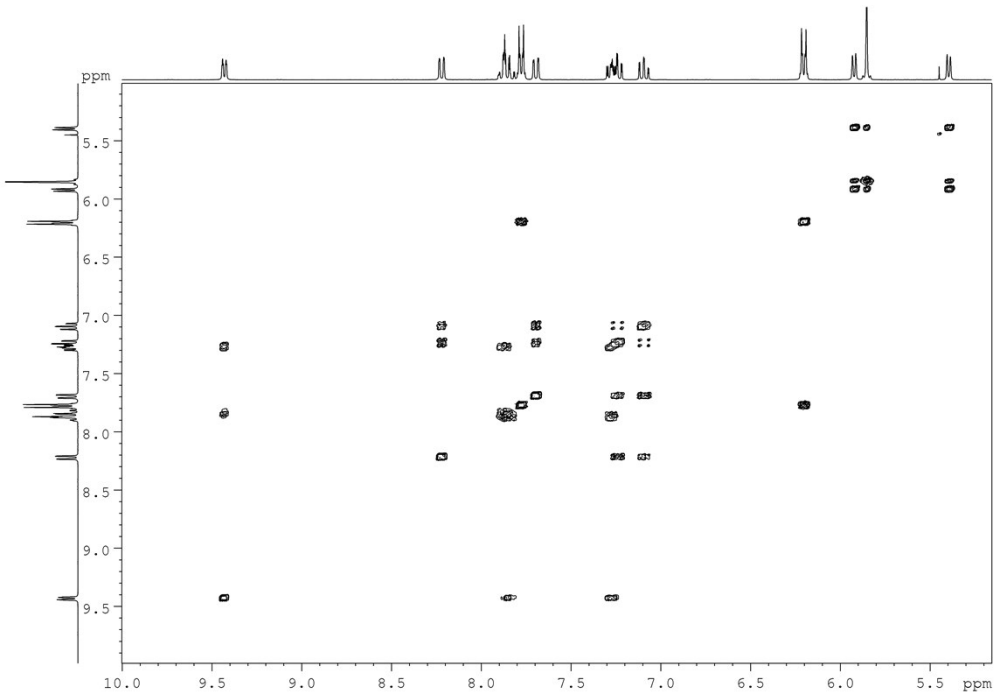

Figure S12. 300 MHz [^{1}H, ^{1}H]-COSY NMR spectrum of complex **2a** in CD_3CN.

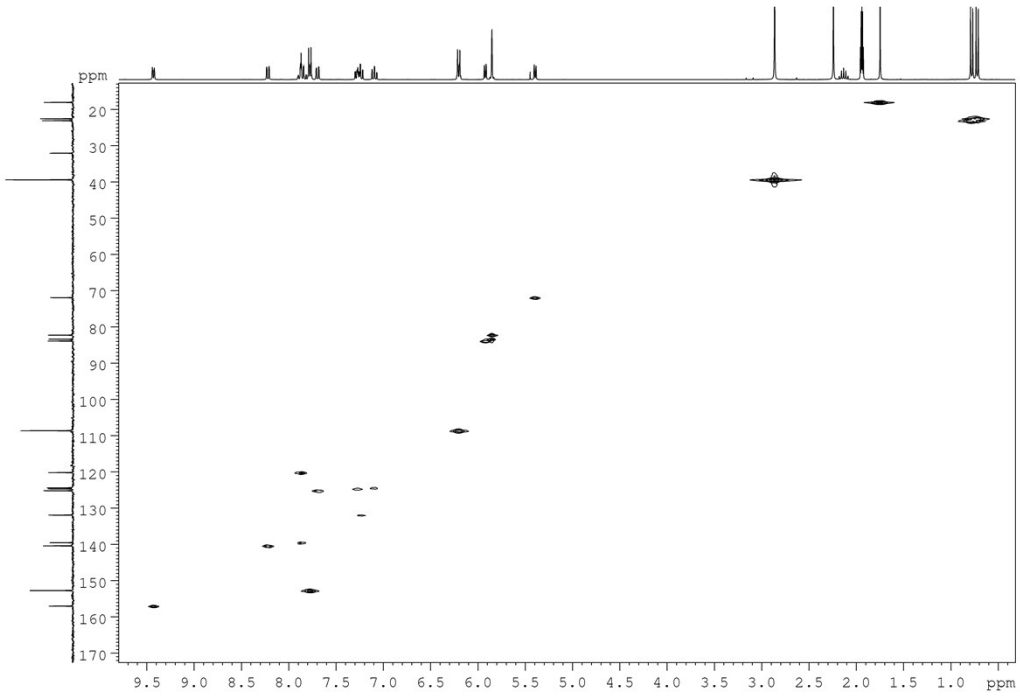

Figure S13. [^{1}H, ^{13}C]-HSQC 2D NMR (^{1}H, 300 MHz) spectrum of complex **2a** in CD_3CN.

Compound 3a

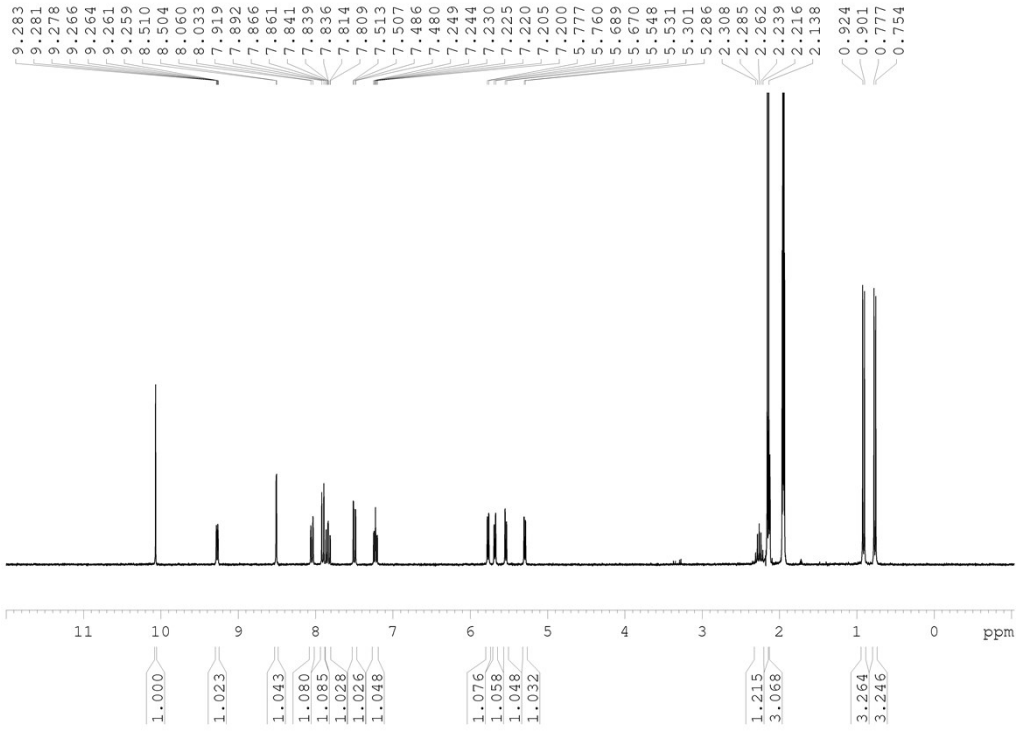

Figure S14. 300 MHz ^{1}H NMR spectrum of complex **3a** in CD_3CN.

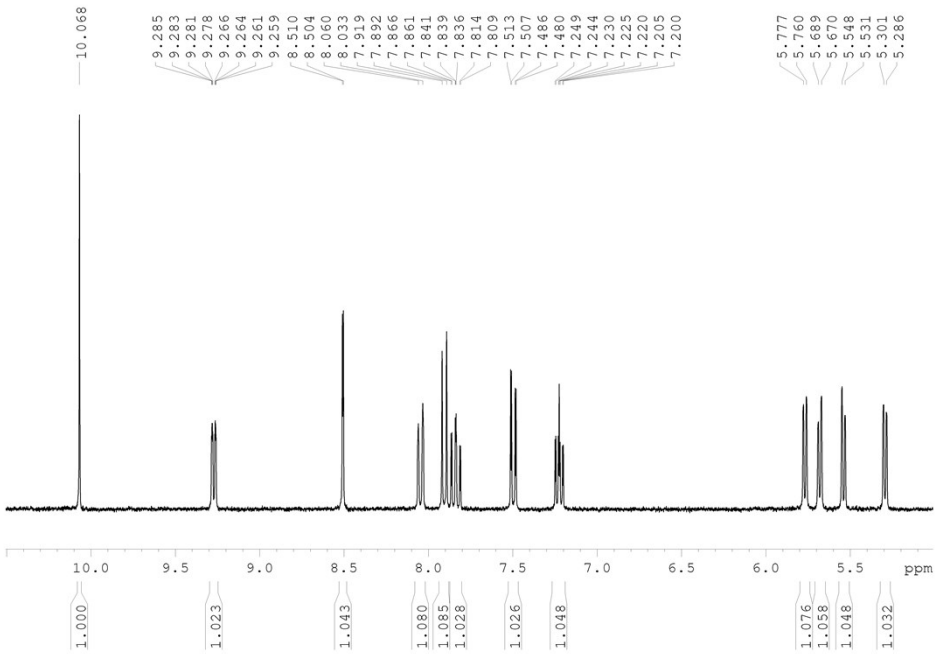

Figure S15. Aromatic region of ^{1}H NMR spectrum of complex **3a** in CD_3CN.

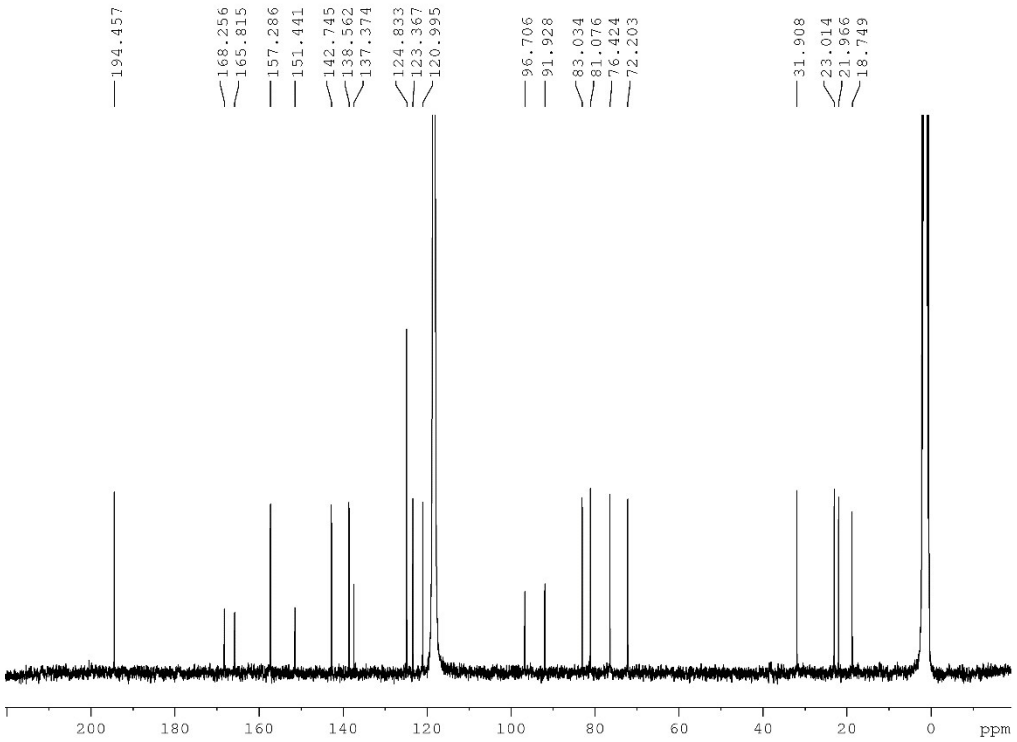

Figure S16. 75 MHz ^{13}C NMR spectrum of complex **3a** in CD_3CN.

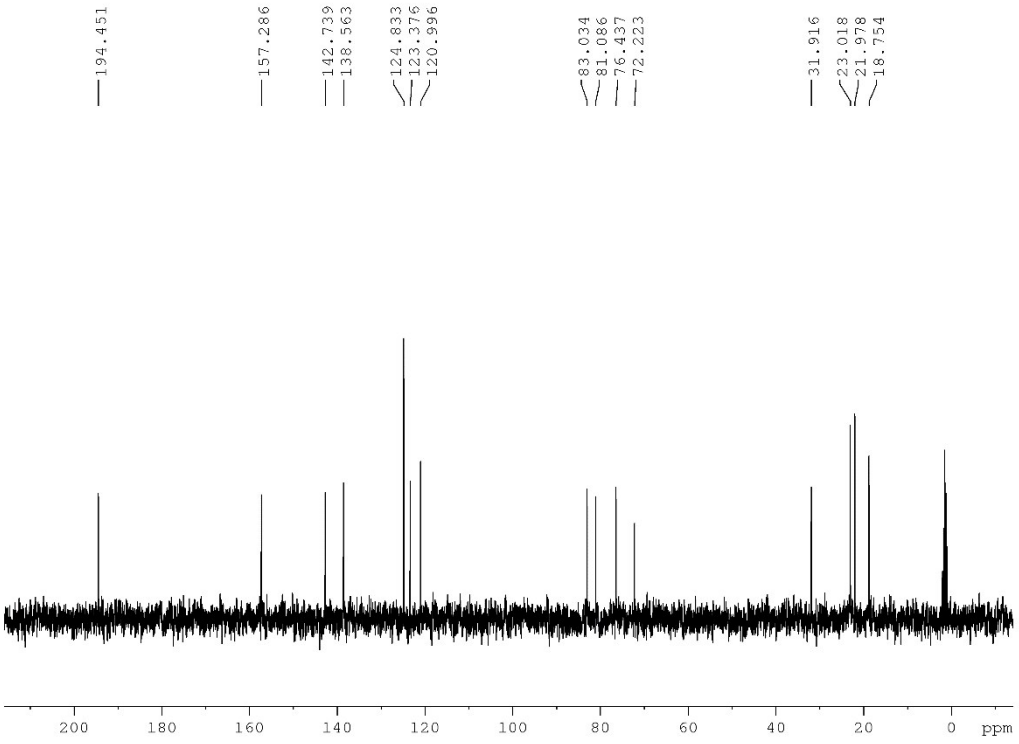

Figure S17. 75 MHz DEPT-135 NMR spectrum of complex **3a** in CD_3CN.

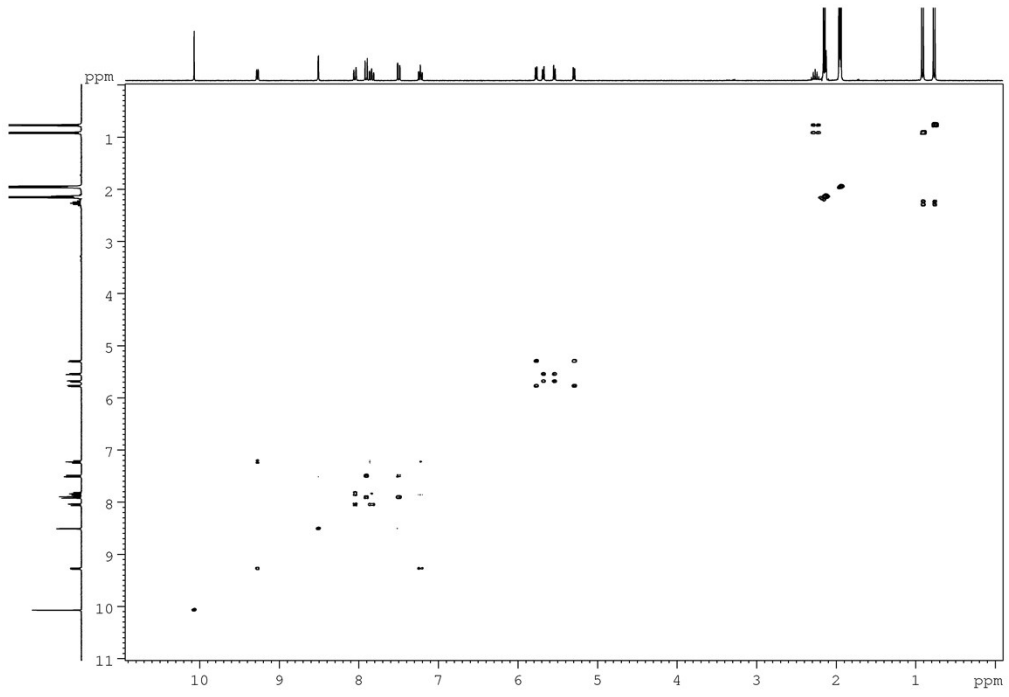

Figure S18. 300 MHz [^{1}H, ^{1}H]-COSY NMR spectrum of complex **3a** in CD_3CN.

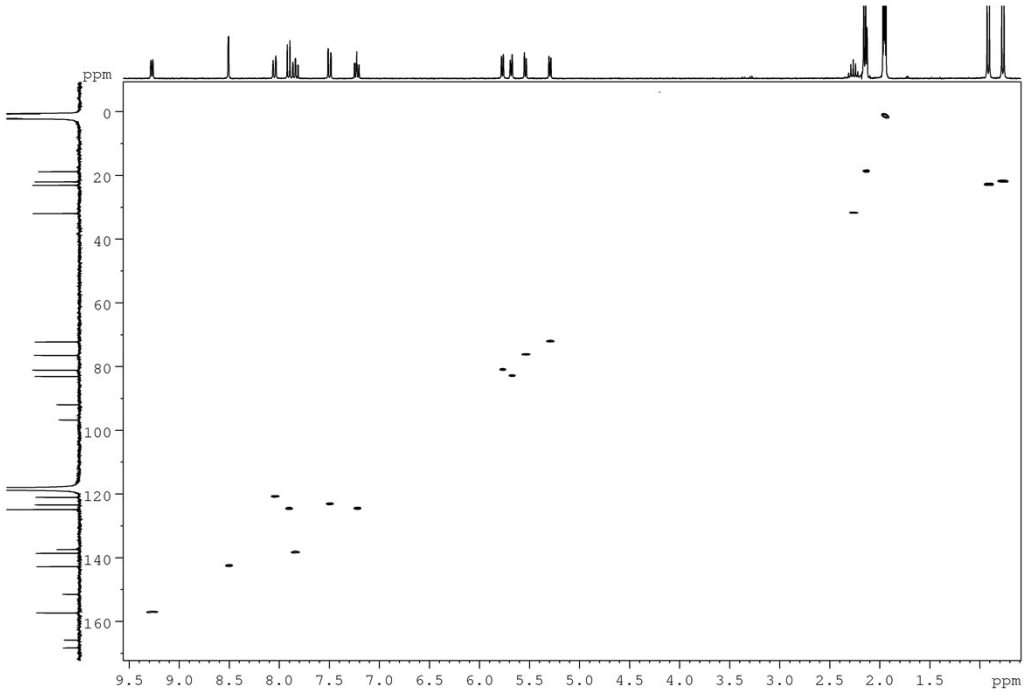

Figure S19. [^{1}H, ^{13}C]-HSQC 2D NMR (^{1}H, 300 MHz) spectrum of complex **3a** in CD_3CN.

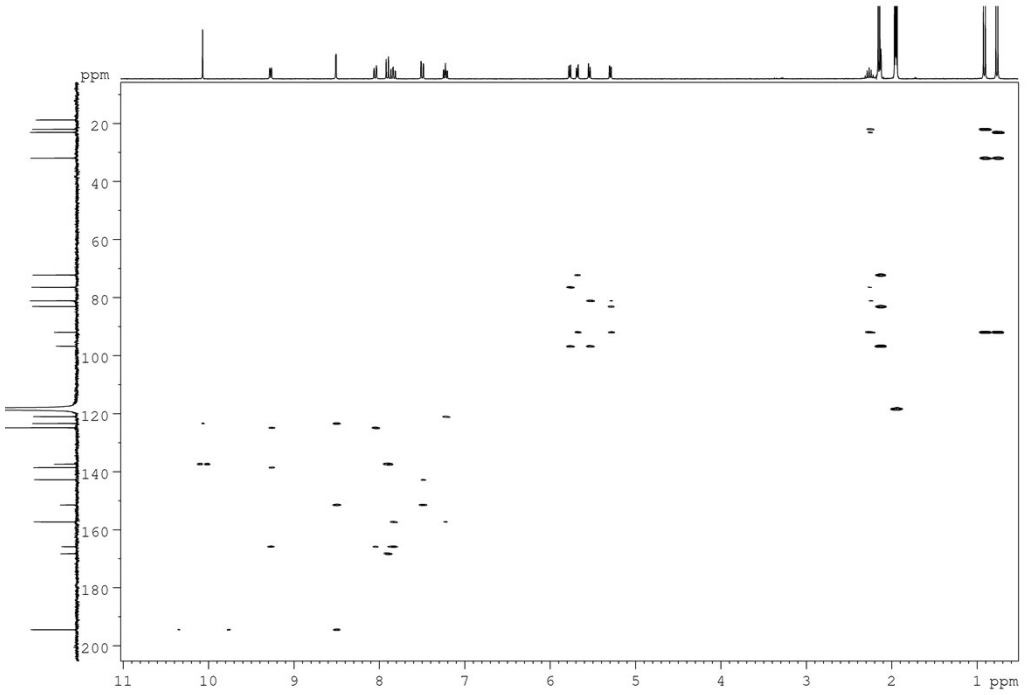

Figure S20. [^{1}H, ^{13}C]-HMBC 2D NMR (^{1}H, 300 MHz) spectrum of complex **3a** in CD_3CN.

Compound 4a

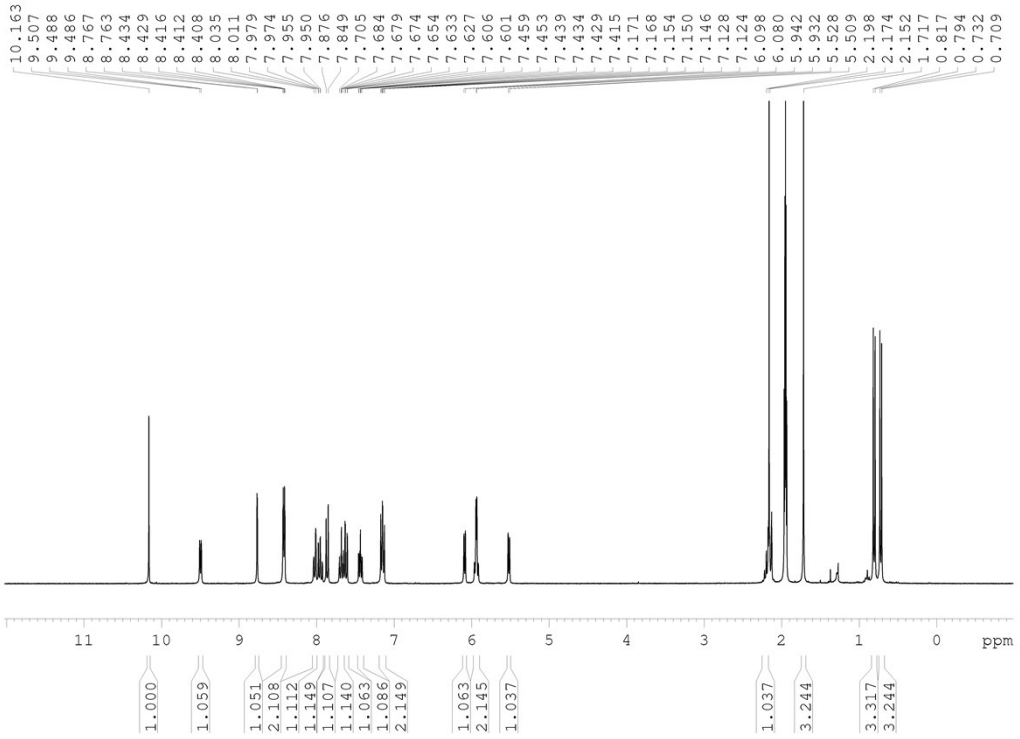

Figure S21. 300 MHz ^{1}H NMR spectrum of complex **4a** in CD_3CN.

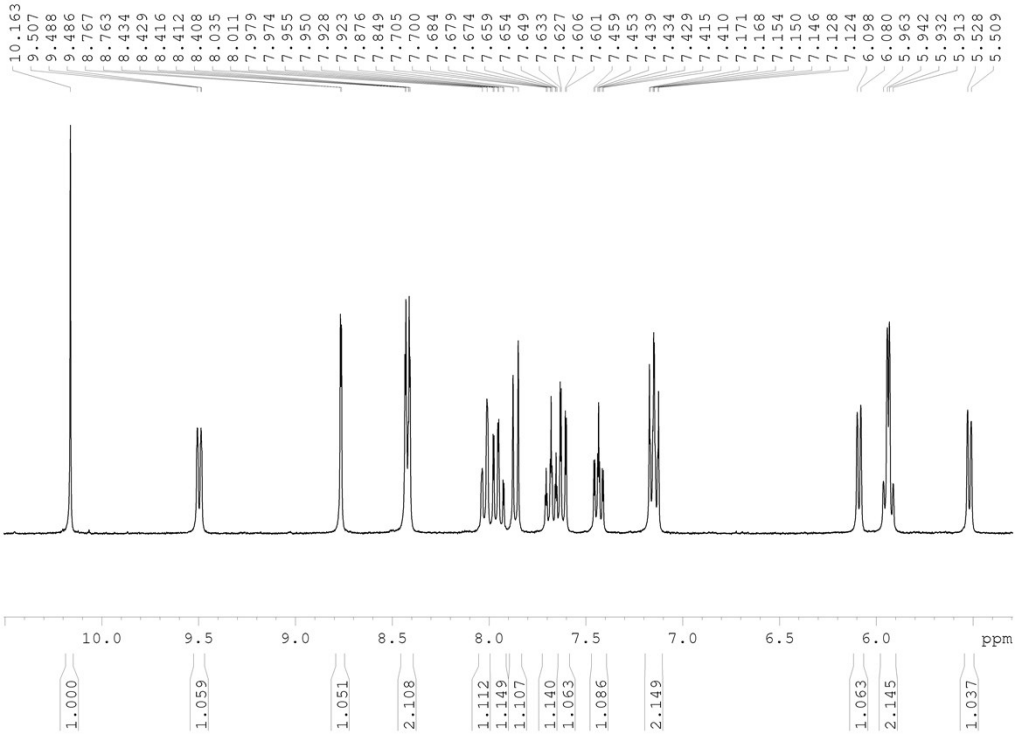

Figure S22. Aromatic region of ^{1}H NMR spectrum of complex **4a** in CD_3CN.

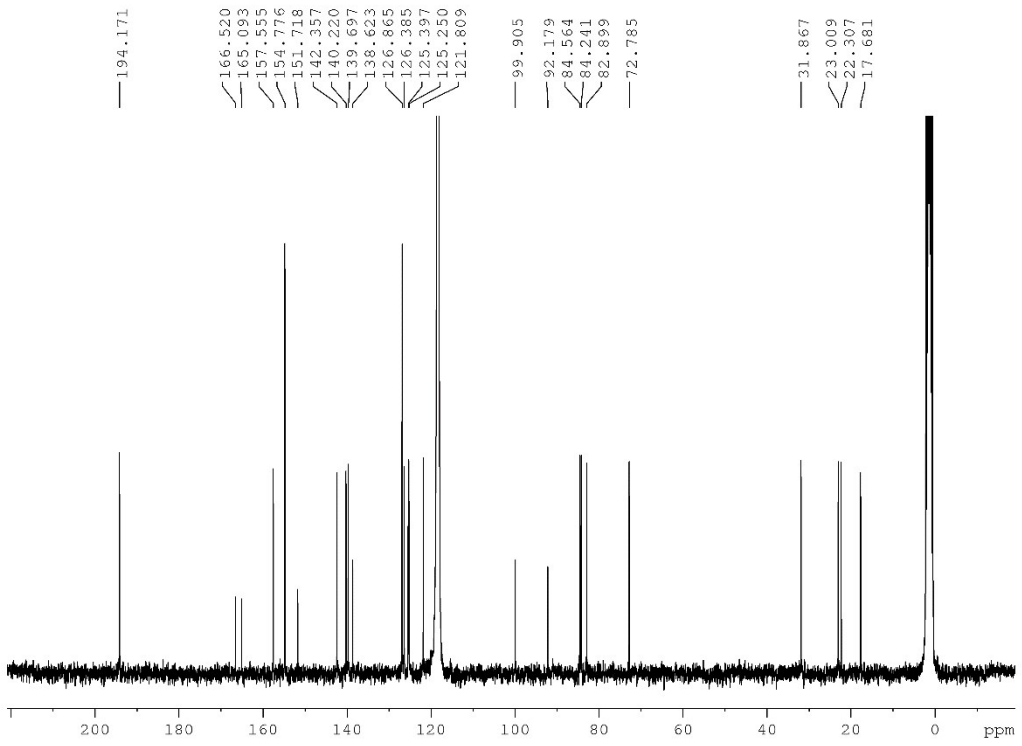

Figure S23. 75 MHz ^{13}C NMR spectrum of complex **4a** in CD_3CN.

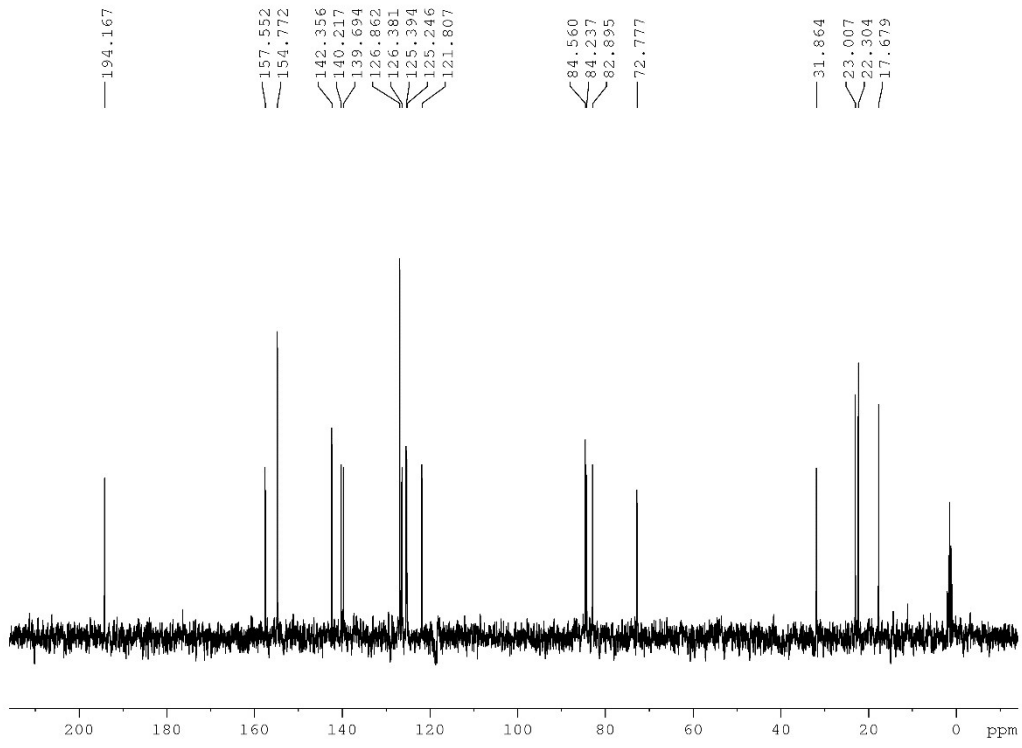

Figure S24. 75 MHz DEPT-135 NMR spectrum of complex **4a** in CD_3CN.

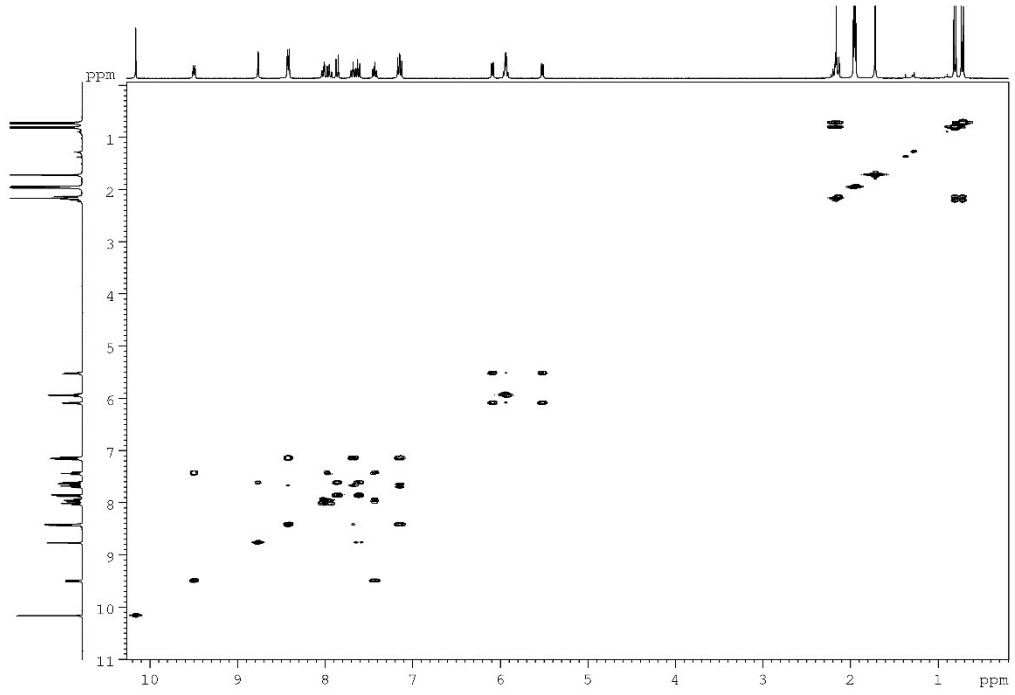

Figure S25. 300 MHz [^{1}H, ^{1}H]-COSY NMR spectrum of complex **4a** in CD_3CN.

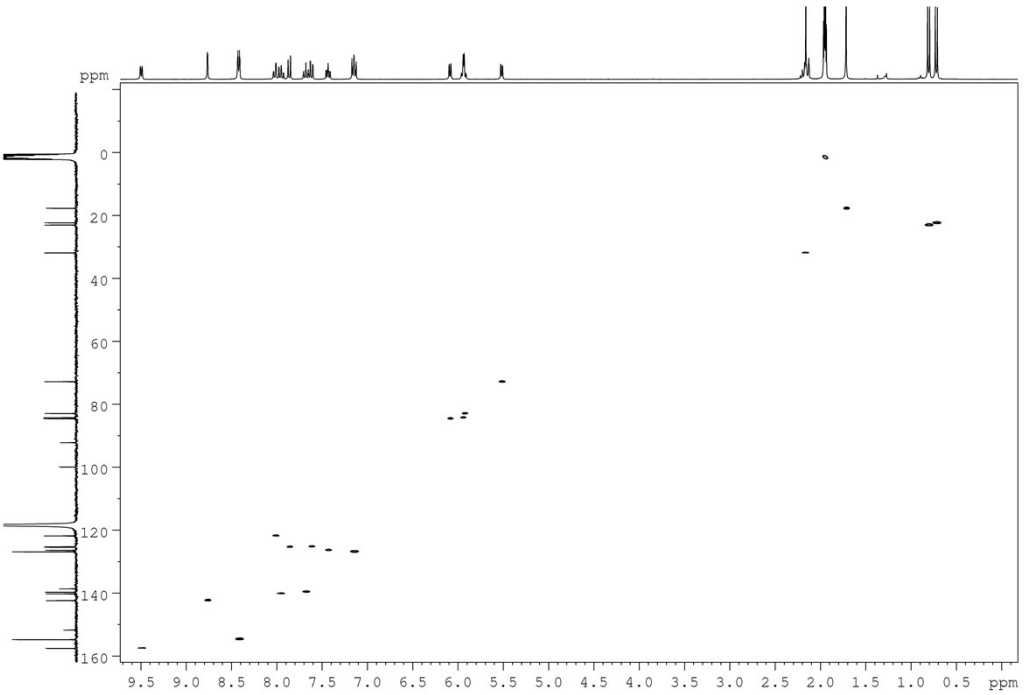

Figure S26. [^{1}H, ^{13}C]-HSQC 2D NMR (^{1}H, 300 MHz) spectrum of complex **4a** in CD_3CN.

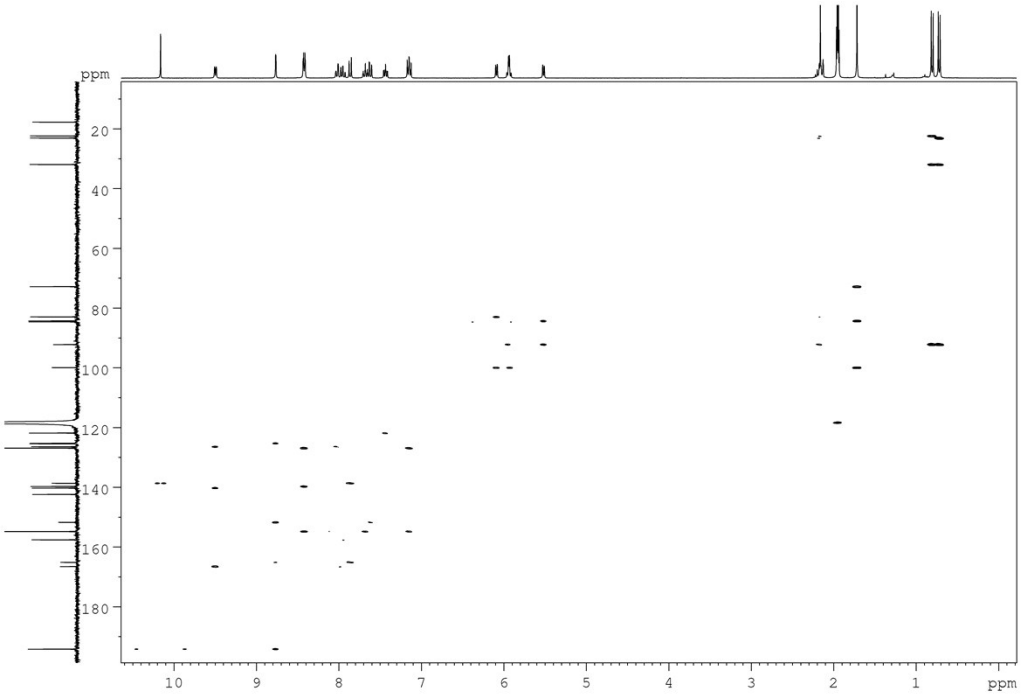

Figure S27. [^{1}H, ^{13}C]-HMBC 2D NMR (^{1}H, 300 MHz) spectrum of complex **4a** in CD_3CN.

Compound 5a

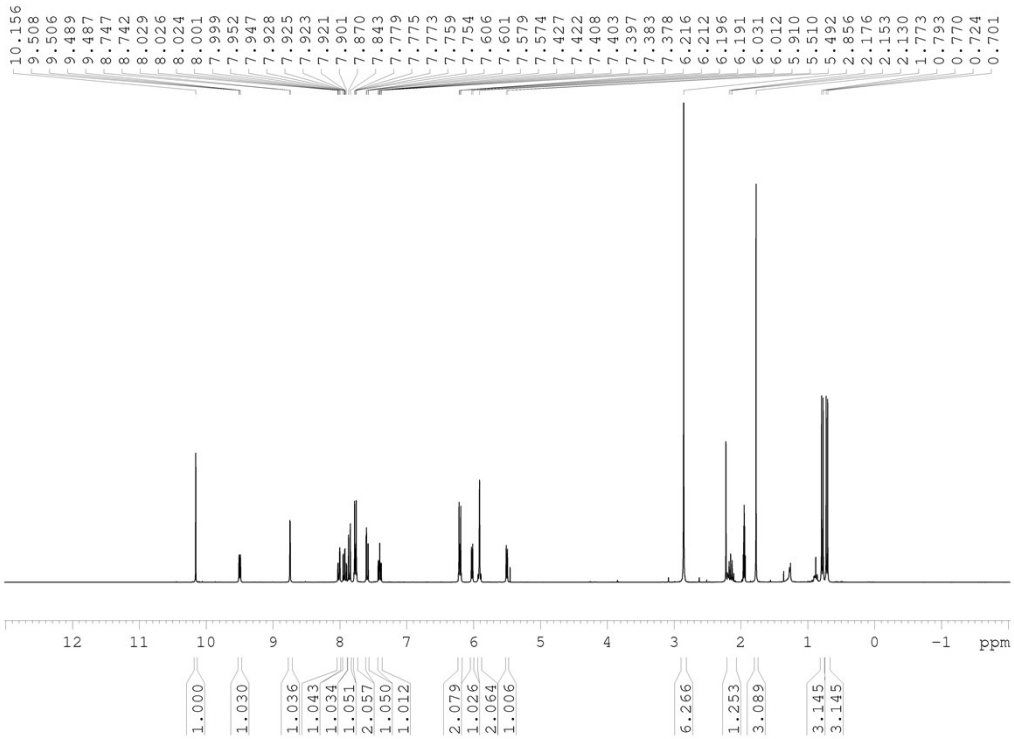

Figure S28. 300 MHz ^{1}H NMR spectrum of complex **5a** in CD_3CN.

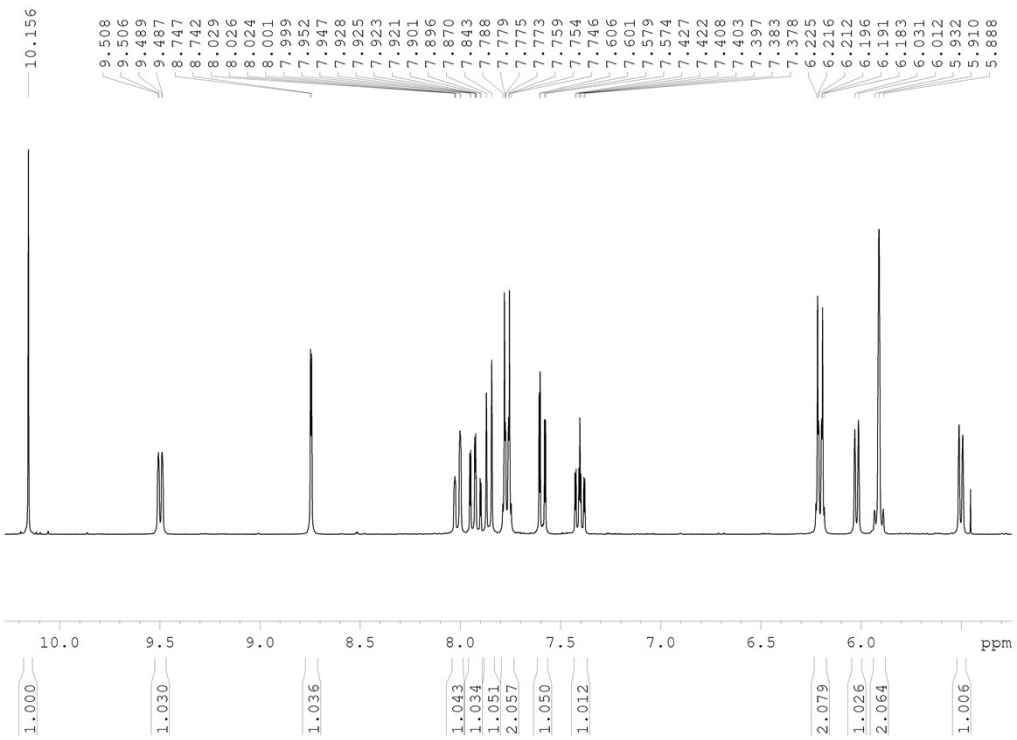

Figure S29. Aromatic region of ^{1}H NMR spectrum of complex **5a** in CD_3CN.

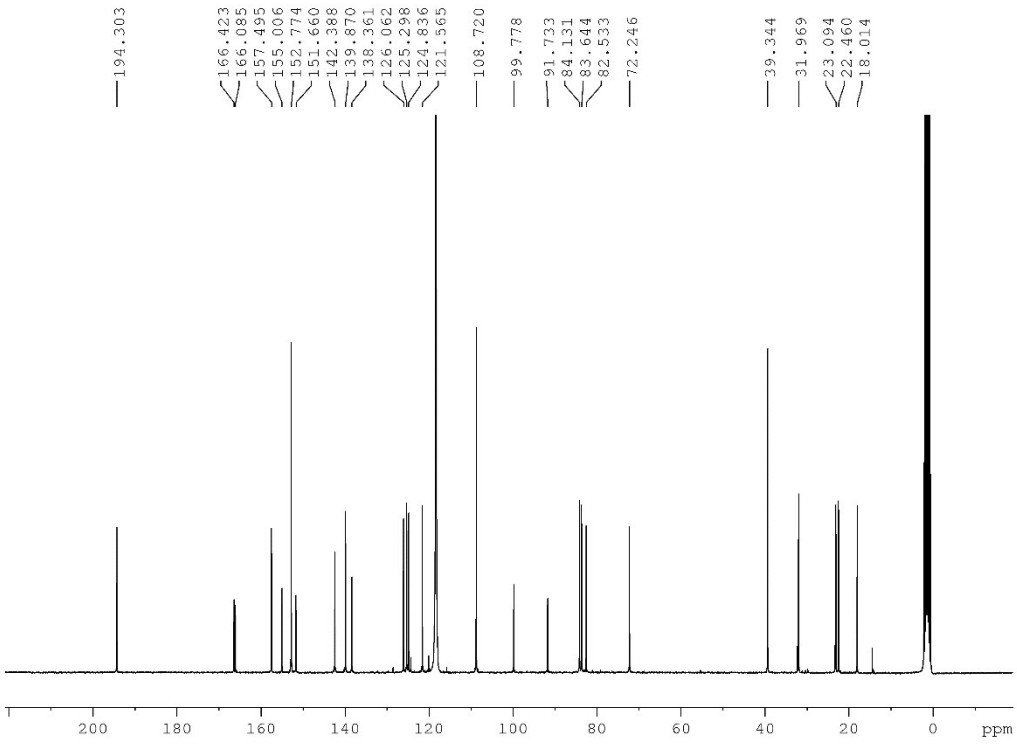

Figure S30. 75 MHz ^{13}C NMR spectrum of complex **5a** in CD_3CN.

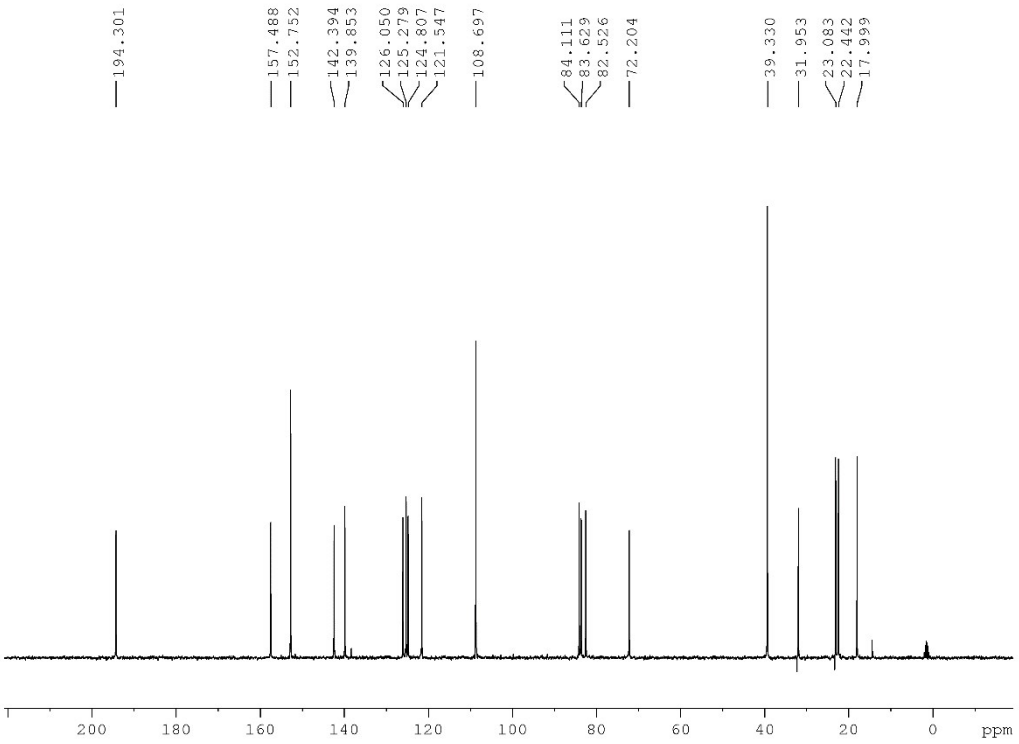

Figure S31. 75 MHz DEPT-135 NMR spectrum of complex **5a** in CD_3CN.

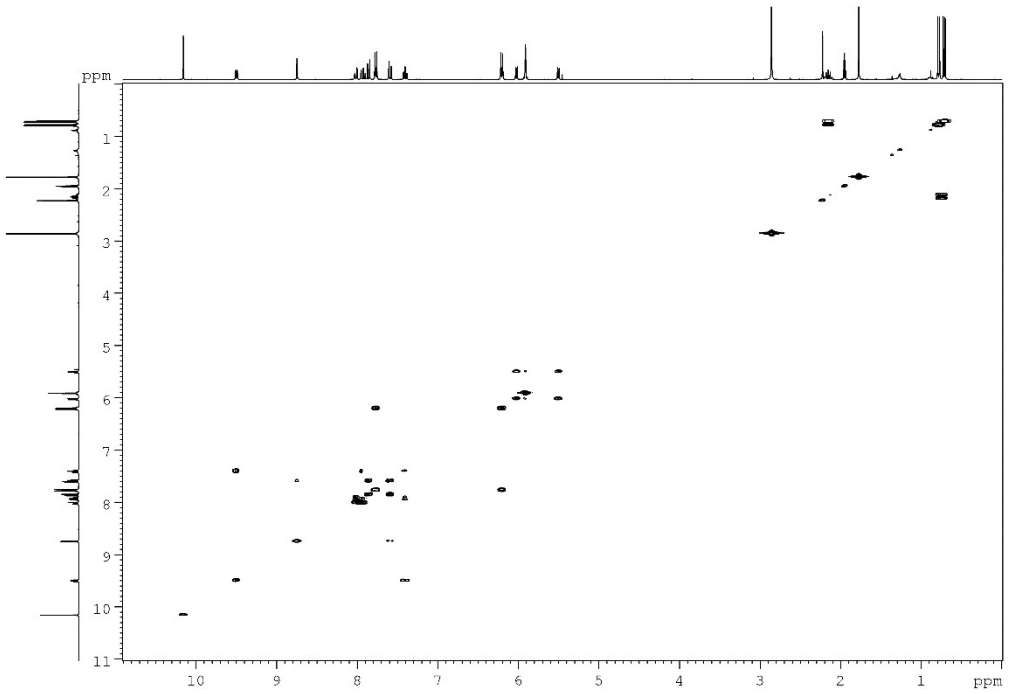

Figure S32. 300 MHz [^{1}H, ^{1}H]-COSY NMR spectrum of complex **5a** in CD_3CN.

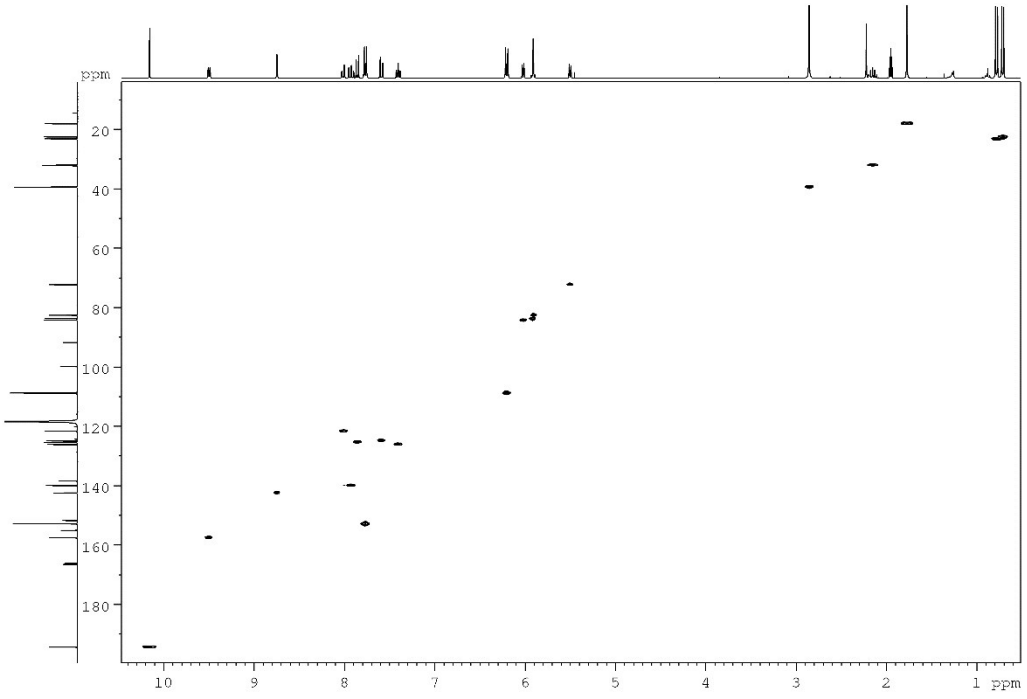

Figure S33. [^{1}H, ^{13}C]-HSQC 2D NMR (^{1}H, 300 MHz) spectrum of complex **5a** in CD_3CN.

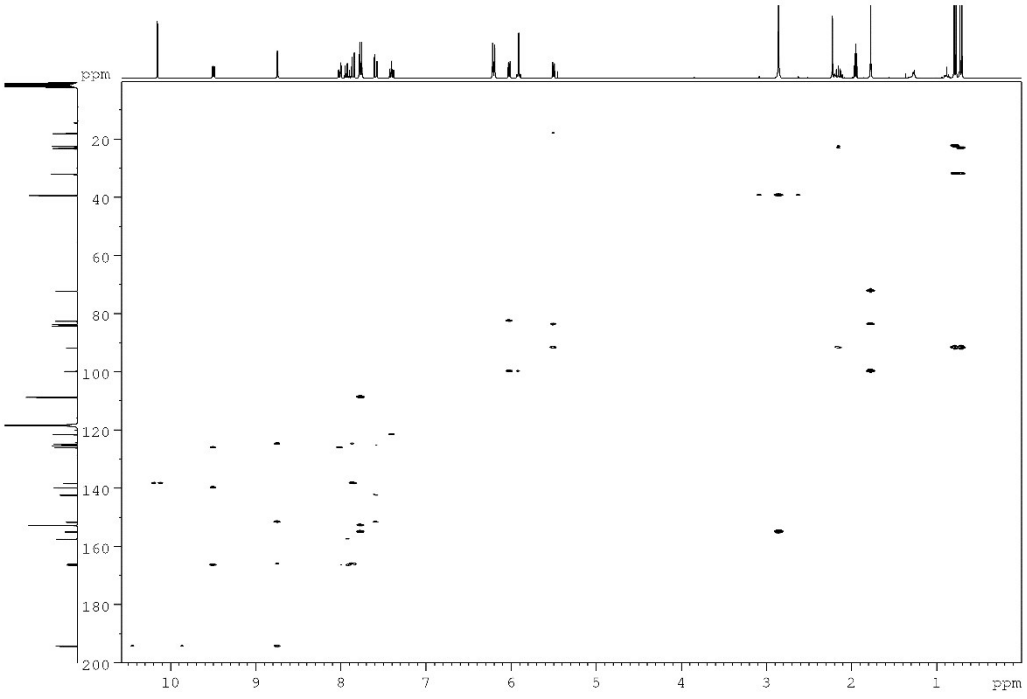

Figure S34. [^{1}H, ^{13}C]-HMBC 2D NMR (^{1}H, 300 MHz) spectrum of complex **5a** in CD_3CN.

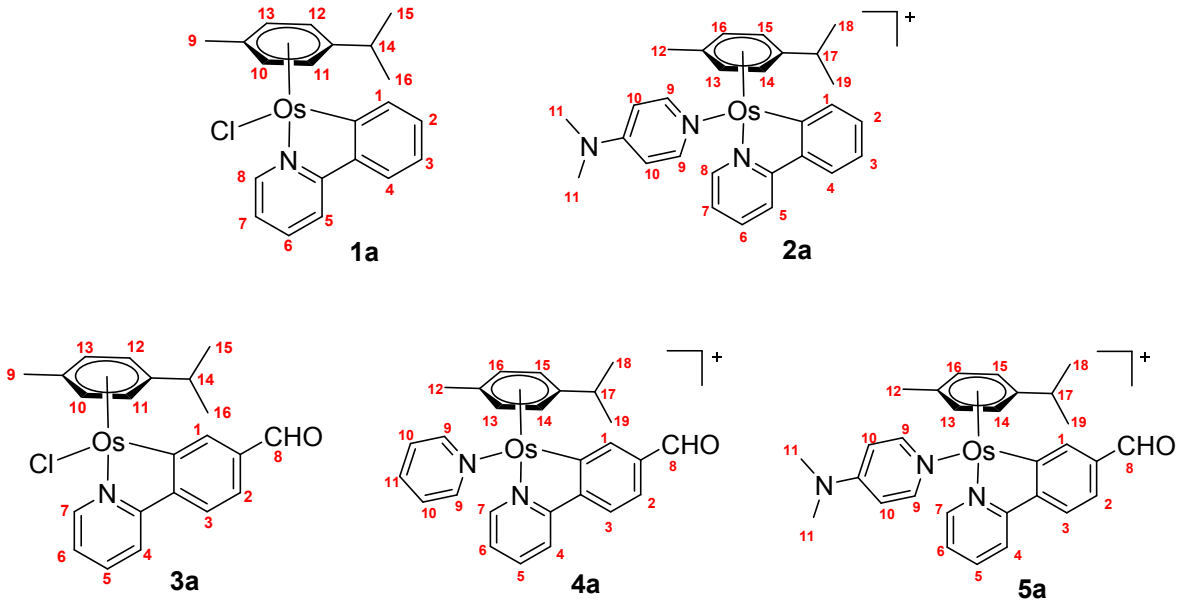

Figure S35. Proton numeration of compounds **1a-5a** used in the signal ^{1}H-NMR assignation.

5. Absorption and emission spectra of complexes 1a-5a

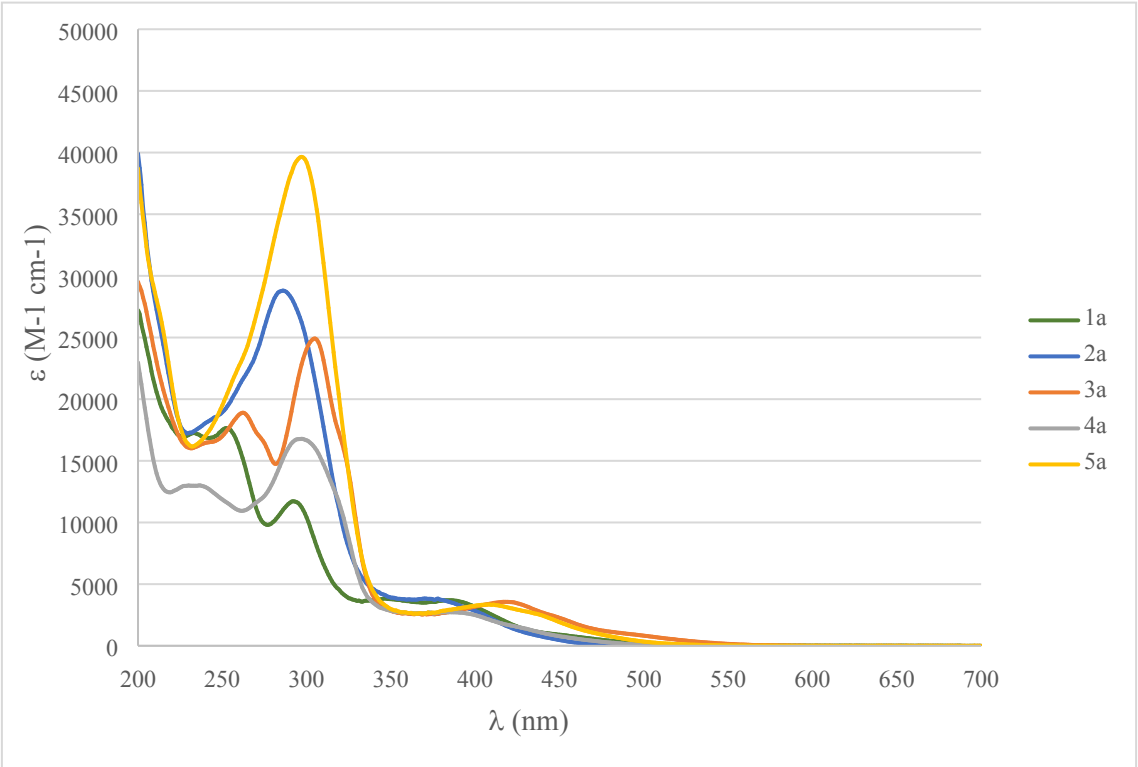

Figure S36. Absorption spectra of complexes **1a-5a** in CD_3CN at 25 ºC.

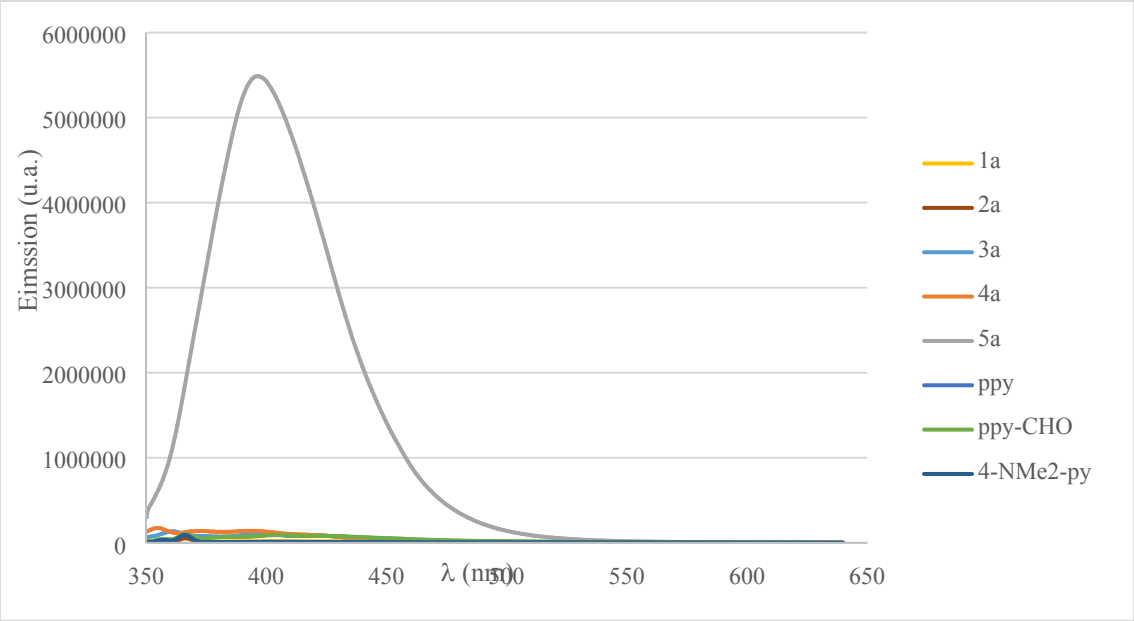

Figure S37. Emission spectra (λ_{ex} = 330 nm) of complexes **1a-5a**, and ligands and proligands at 50 μM in CD_3CN at 25 ºC.

6. UV-VIS stability study of compounds 1a and 2a

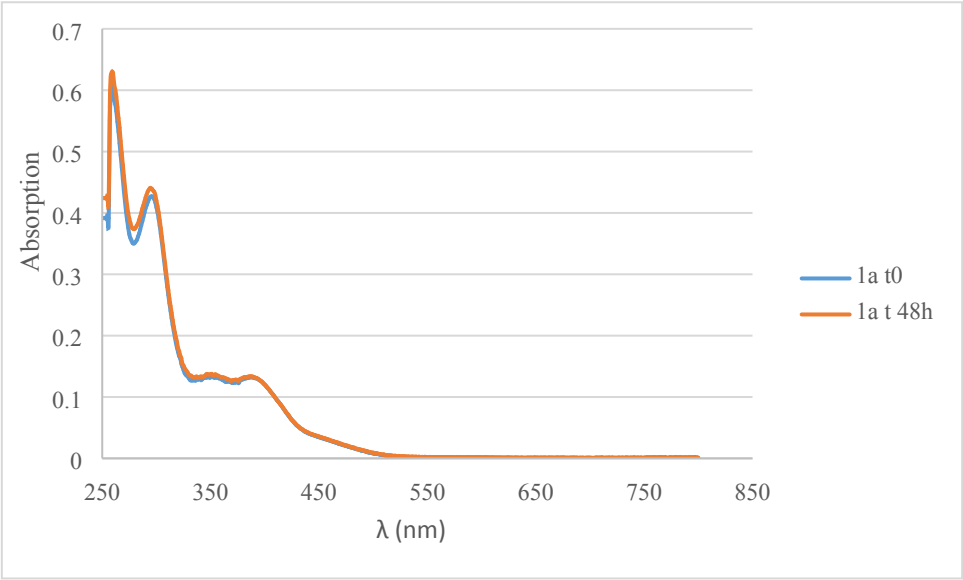

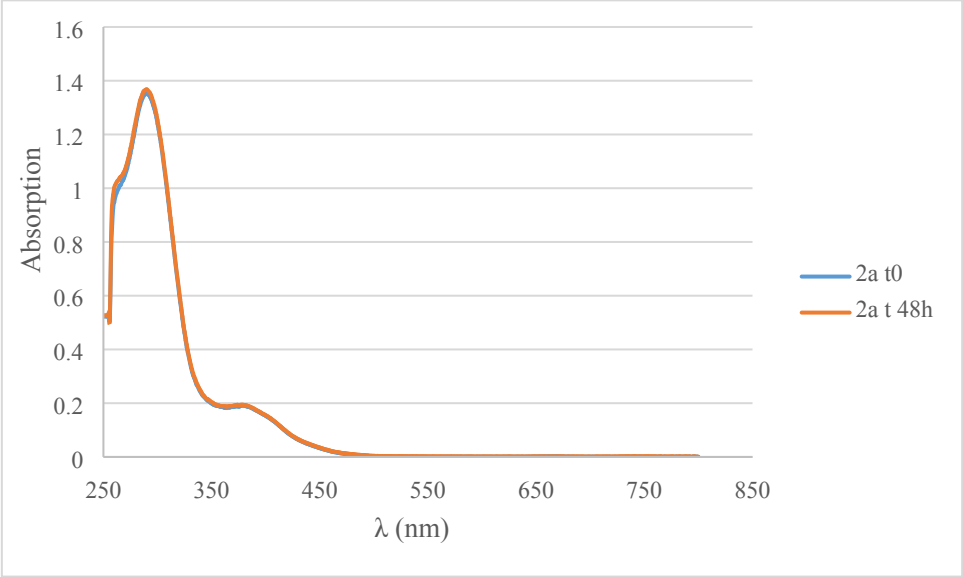

Figure S38. UV-VIS spectra of complexes **1a** (up) and **2a** (down) (50 µM in DMSO) at t = 0 h and after incubation at 37 ºC for 48 hours.

7. HPLC-MS stability studies of compounds 3a-5a

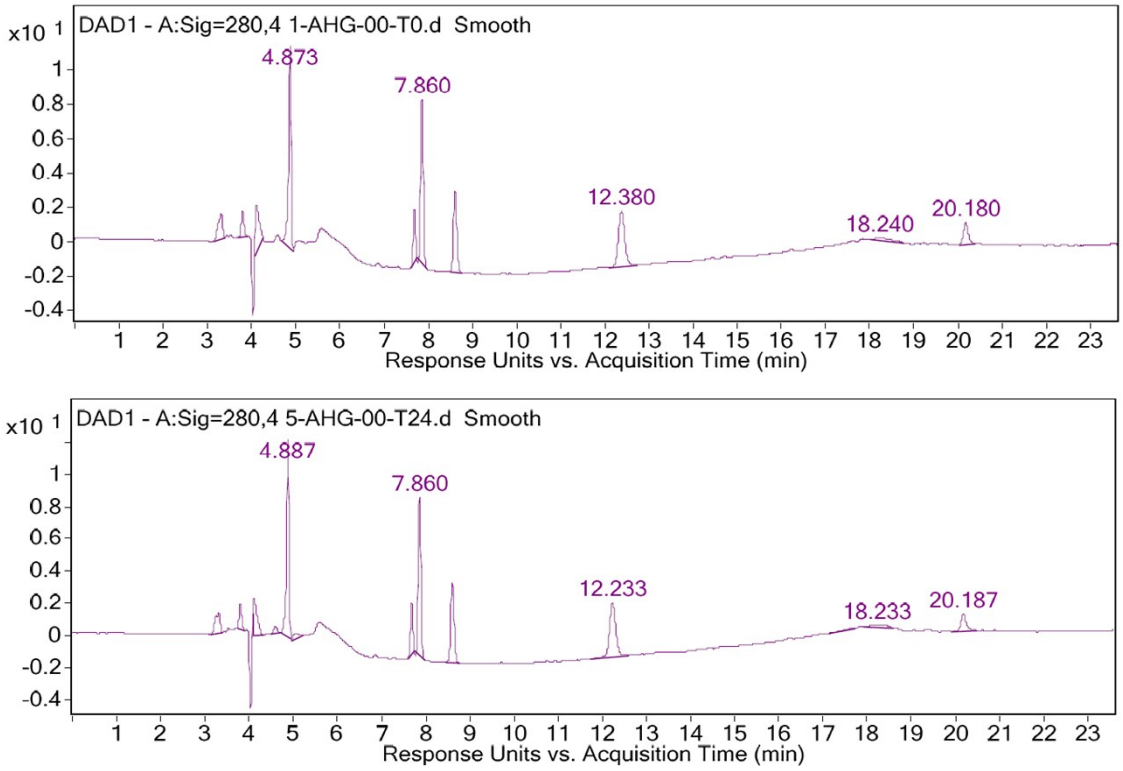

Figure S39. HPLC chromatograms of RPMI medium with 5% of DMSO. Top: t = 0 h. Botton: t= 24 h.

Complex 3a

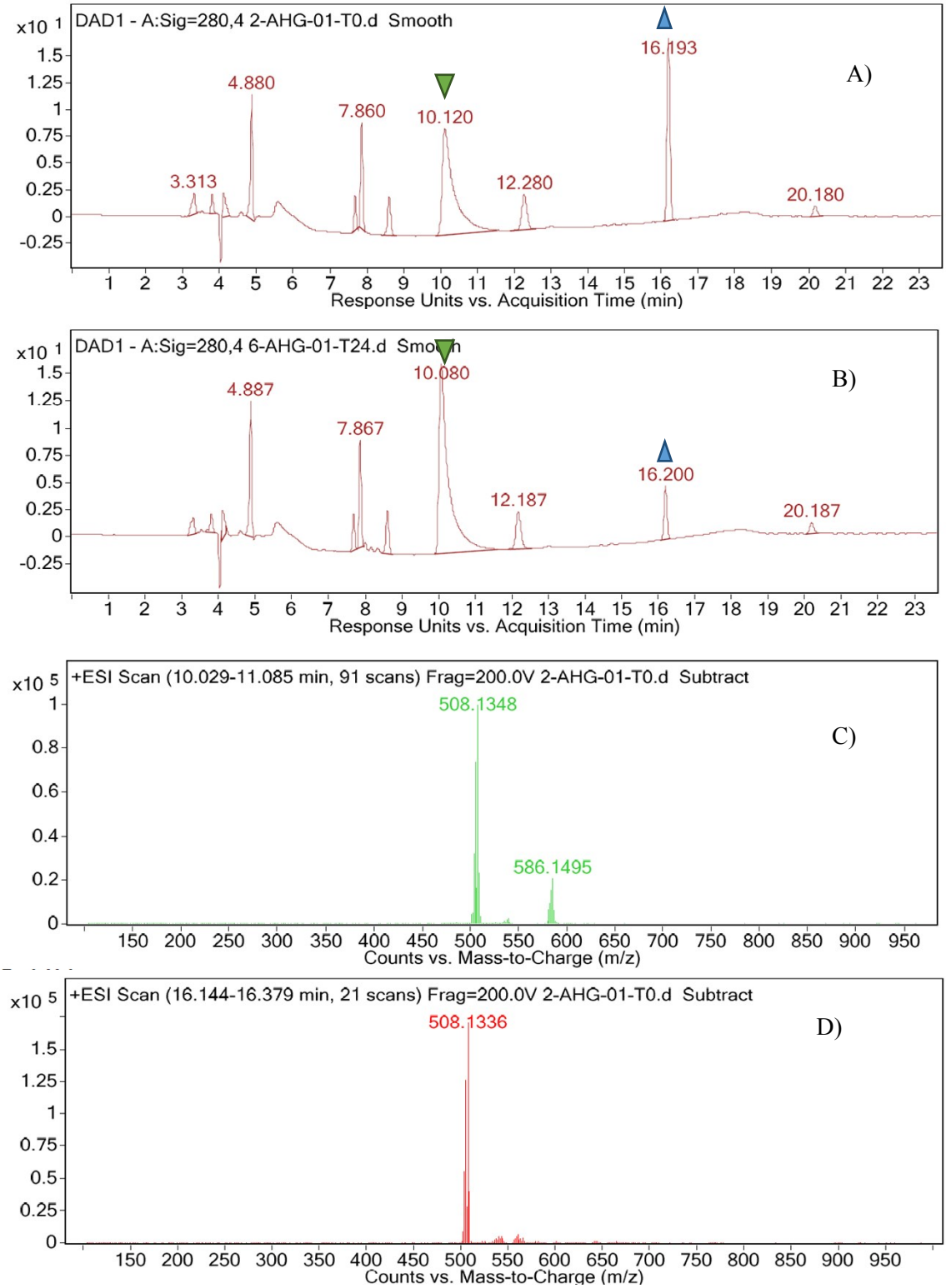

Figure S40. A) HPLC chromatogram of RPMI medium with compound **3a** in 5% of DMSO at t = 0 h. B) HPLC chromatogram of RPMI medium with compound **3a** in 5% of DMSO after incubation at 37ºC during 24 h. C) ESI-MS of the peak with t_R=10 min related to the DMSO-Complex **3a** ▼. D) ESI-MS of the peak with t_R=16 min related to the Complex **3a** ▲

Complex 4a

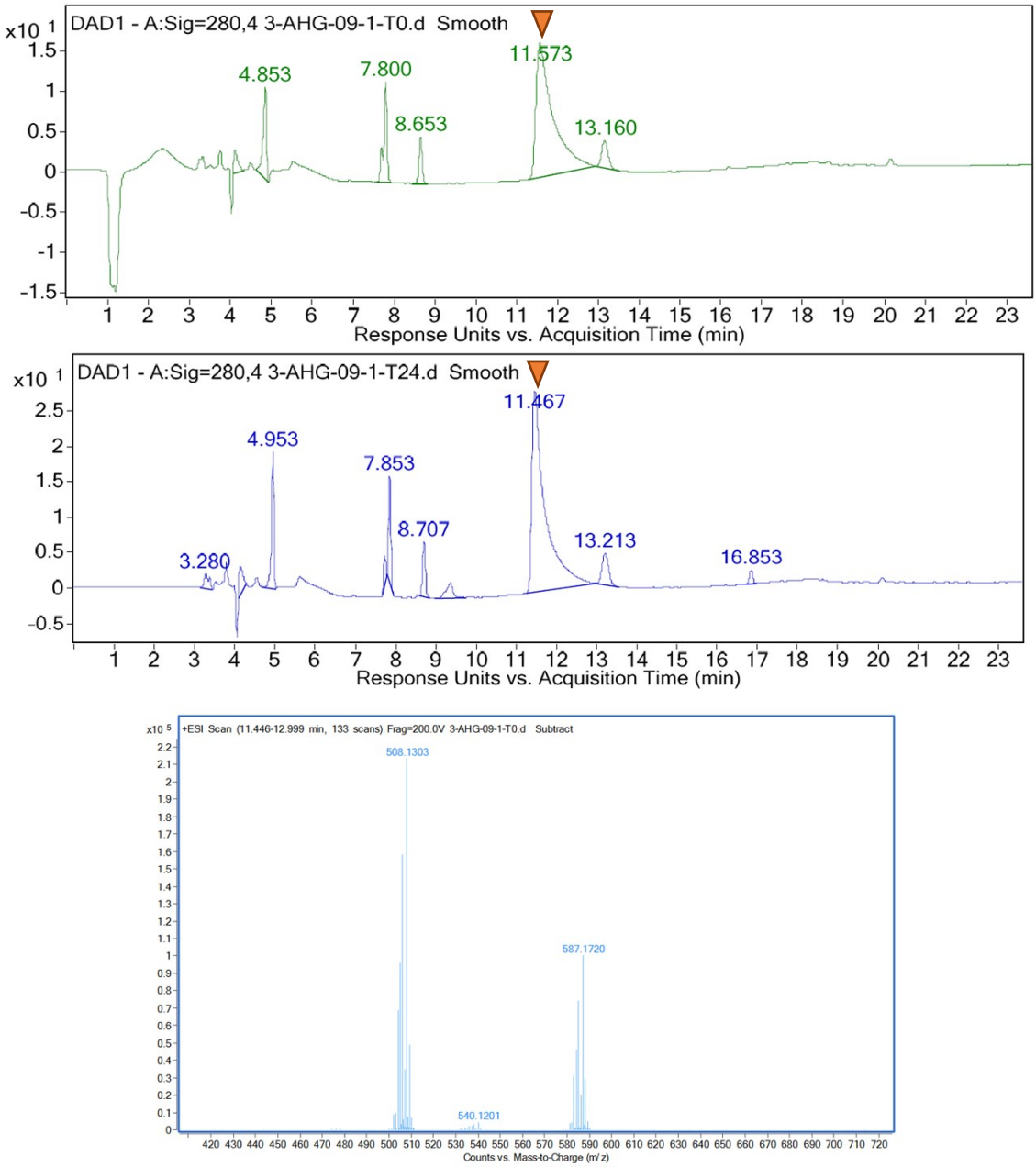

Figure S41. Top: HPLC chromatogram of RPMI medium with compound **4a** in 5% of DMSO at t = 0 h. Middel: HPLC chromatogram of RPMI medium with compound **4a** in 5% of DMSO after incubation at 37ºC during 24 h. Bottom: ESI-MS of the peak with t_R=11 min related to the Complex **4a** ▼.

Complex 5a

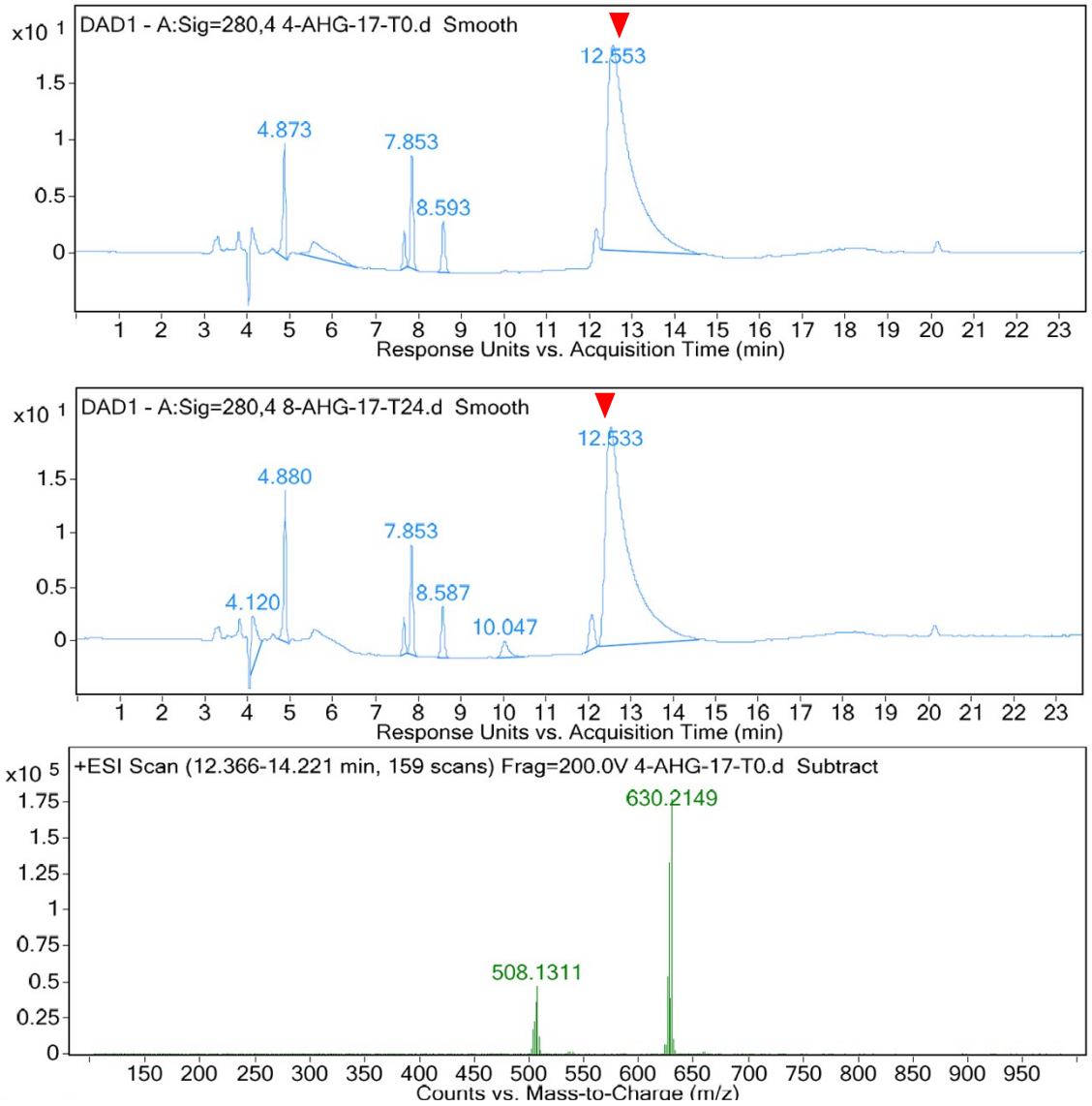

Figure S42. Top: HPLC chromatogram of RPMI medium with compound **5a** in 5% of DMSO at t = 0 h. Middel: HPLC chromatogram of RPMI medium with compound **5a** in 5% of DMSO after incubation at 37ºC during 24 h. Bottom: ESI-MS of the peak with t_R=11 min related to the Complex **5a** ▼.

8. Hydrolysis of complex 3a

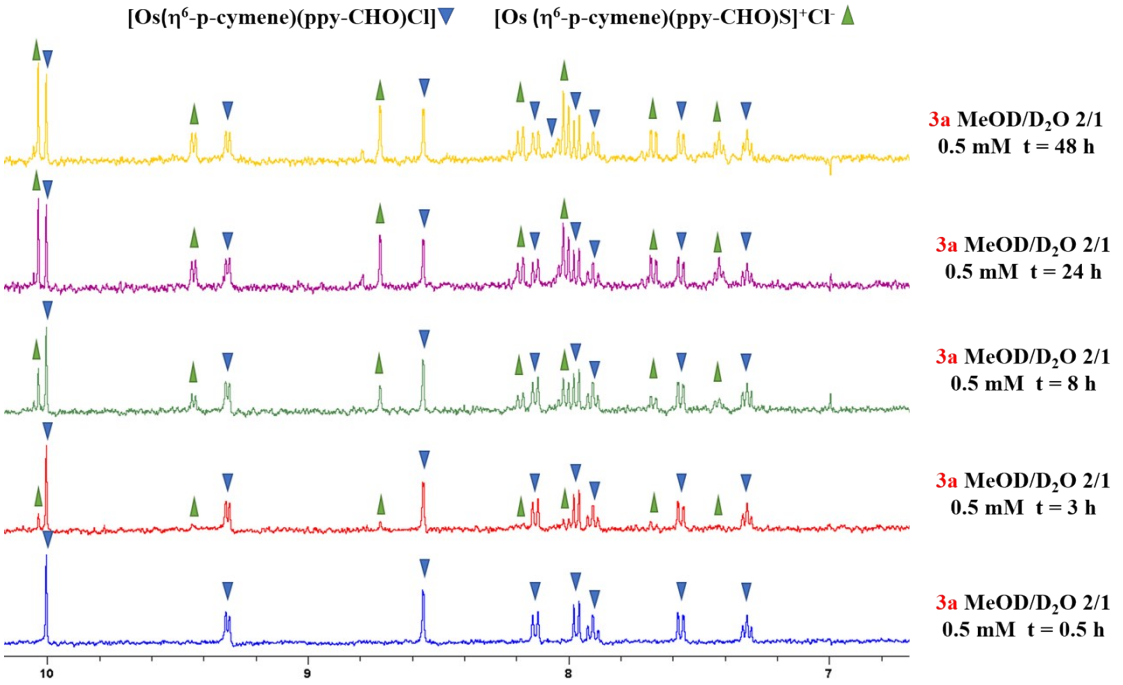

Figure S43. ^{1}H-NMR spectra of compound **3a** (0.5 mM in 600 µL of mixture of 2/1 methanol and deuterated water) after different times ▲:[Os(η^6-p-cymene)(ppy-CHO)Cl] and ▼:[Os(η^6-p-cymene)(ppy-CHO)(OH_2)]$^+$.

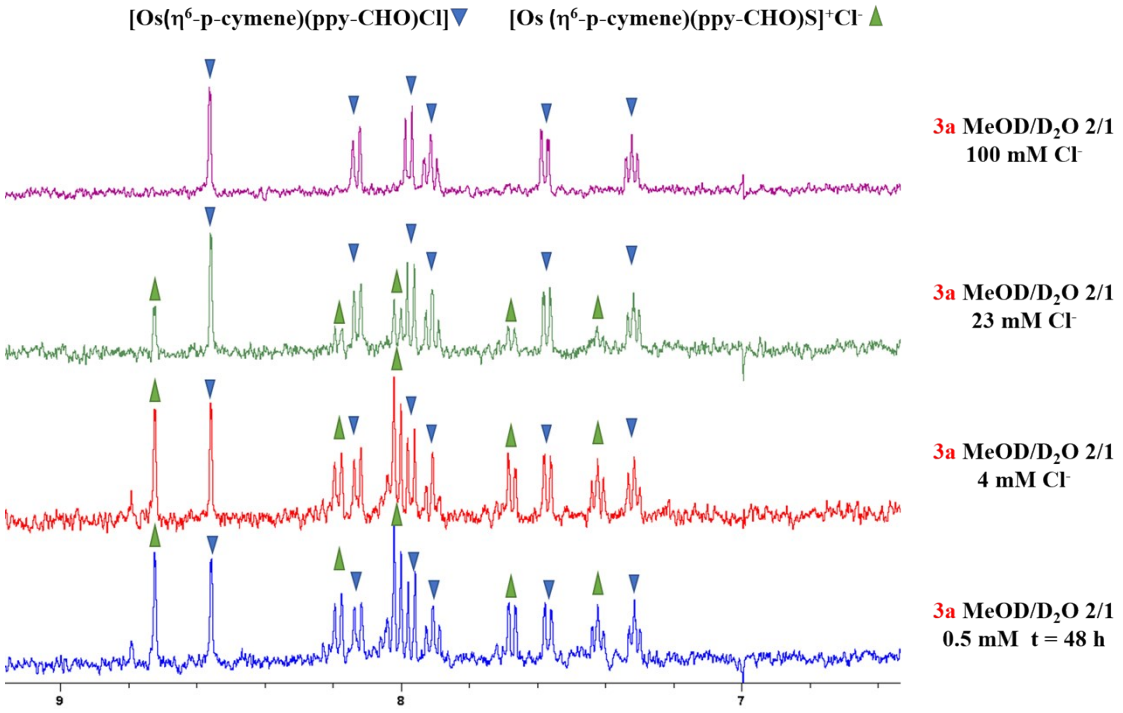

Figure S44. ^{1}H-NMR spectra of compound **3a** (0.5 mM in 600 µL of mixture of 2/1 methanol and deuterated water) after 48 hours and with consecutive additions of chloride ion ▲:[Os(η^6-p-cymene)(ppy-CHO)Cl] and ▼:[Os(η^6-p-cymene)(ppy-CHO)(OH_2)]$^+$.

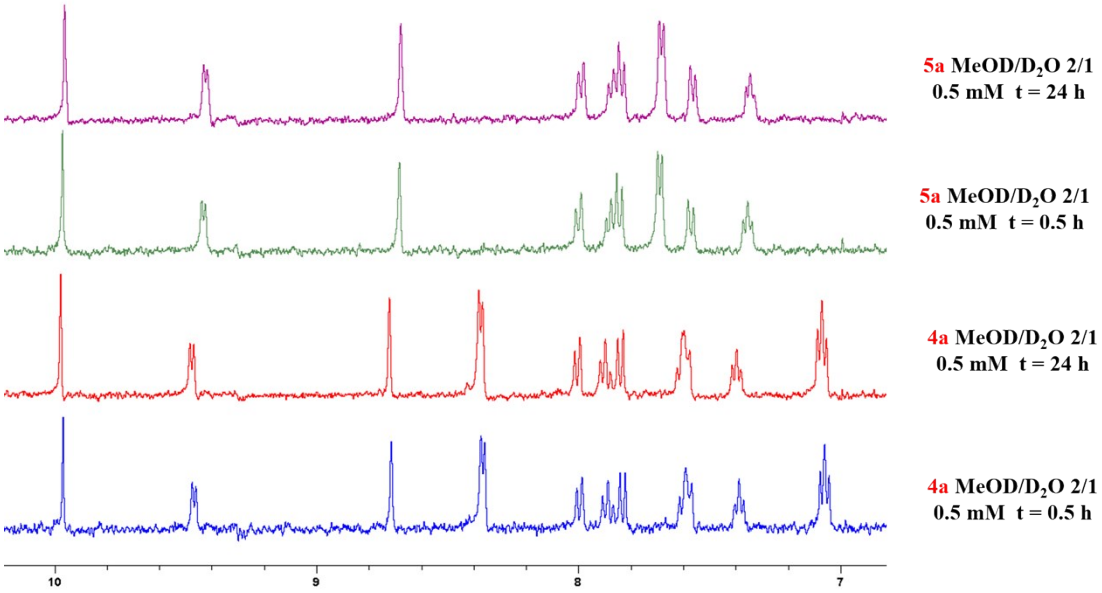

Figure S45. ^{1}H-NMR spectra of compound **4a** and **5a** (0.5 mM in 600 μL of mixture of 2/1 methanol and deuterated water) at different times.

9. X-Ray structures of compounds 3a-5a

Special features: Compound **4a**: The triflate anion is disordered over two positions.

Table S1. Crystal data and structure refinement for complexes **3a**, **4a** and **5a**

Complex	**3a**	**4a**	**5a**
Empirical formula	$C_{22}H_{22}ClNOOs$	$C_{28}H_{27}F_3N_2O_4OsS$	$C_{30}H_{32}F_3N_3O_4OsS$
Formula weight	542.05	734.77	777.84
Temperature/ K	100(2)	100(2)	100(2)
Wavelength/ Å	0.71073	0.71073	0.71073
Crystal system	Monoclinic	Monoclinic	Monoclinic
Space group	$P2_1/n$	$P2_1/n$	$P2_1/n$
Unit cell dimensions			
a/ Å	11.1387(4)	12.1045(5)	11.4840(6)
b/ Å	13.1760(5)	16.9592(7)	14.3590(8)
c/ Å	12.5063(5)	12.9824(6)	17.8290(10)
α/ °	90	90	90
β/ °	91.3700(10)	92.737(2)	96.510(2)
γ /°	90	90	90
Volume/ $Å^3$	1834.94(12)	2662.0(2)	2921.0(3)
Z	4	4	4
$Density_{calculated}$/ Mg/m^3	1.962	1.833	1.769
Absorption coefficient/ mm^{-1}	7.106	4.928	4.497
F(000)	1048	1440	1536
Crystal size/ mm^3	0.330 x 0.250 x 0.210	0.300 x 0.300 x 0.140	0.260 x 0.240 x 0.050
Theta range for data collection/°	2.246 to 30.609	1.977 to 30.568	1.826 to 27.101
Index ranges	-15 ≤ h ≤ 15 -18 ≤ k ≤ 18 -17 ≤ l ≤ 17	-17 ≤ h ≤ 16 -24 ≤ k ≤ 22 -18 ≤ l ≤18	-14 ≤ h ≤ 14 -18 ≤ k ≤ 18 -22 ≤ l ≤ 22
Reflections collected	120198	29336	113650
Independent reflections	5630 [R_{int} = 0.0385]	8132 [R_{int} = 0.0378]	6447 [R_{int} = 0.0345]
Completeness to theta = 25.242°	100.0 %	100.0 %	100.0 %
Absorption correction	Semi-empirical from equivalents	Semi-empirical from equivalents	Semi-empirical from equivalents
Max. and min. transmission	0.7461 and 0.4511	0.7461 and 0.4489	0.7461 and 0.4737
Refinement method	Full-matrix least-squares on F^2	Full-matrix least-squares on F^2	Full-matrix least-squares on F^2
Data / restraints / parameters	5630 / 0 / 238	8132 / 84 / 428	6447 / 0 / 384
Goodness-of-fit on F^2	1.202	1.020	1.105
Final R indices [I>2σ(I)]	R1 = 0.0134 wR2 = 0.0323	R1 = 0.0247 wR2 = 0.0509	R1 = 0.0190 wR2 = 0.0384
R indices (all data)	R1 = 0.0146 wR2 = 0.0327	R1 = 0.0341 wR2 = 0.0533	R1 = 0.0223 wR2 = 0.0394
Largest diff. peak and hole/ $e.Å^{-3}$	0.505 and -1.040	0.818 and -1.738	2.011 and -1.133

Table S2. Bond lengths [Å] and angles [°] for complexes **3a**, **4a** and **5a**

	3a	**4a**	**5a**
Os(1)-C(11)	2.0543(15)	2.060(2)	2.055(2)
Os(1)-N(1)	2.0946(14)	2.093(2)	2.089(2)
Os(1)-C(1)	2.1839(16)	2.194(3)	2.212(2)
Os(1)-C(2)	2.1615(17)	2.252(3)	2.176(2)
Os(1)-C(3)	2.1830(17)	2.271(3)	2.204(2)
Os(1)-C(4)	2.2279(17)	2.215(3)	2.224(2)
Os(1)-C(5)	2.2722(16)	2.182(3)	2.266(2)
Os(1)-C(6)	2.2655(16)	2.166(2)	2.186(2)
Os(1)-Cl(1)	2.4281(4)		
Os(1)-N(31)		2.117(2)	
Os(1)-N(23)			2.125(2)
C(11)-Os(1)-N(1)	77.37(6)	77.36(9)	77.39(9)
N(1)-Os(1)-C(1)	91.92(6)	93.10(10)	105.08(8)
N(1)-Os(1)-C(2)	116.09(6)	95.66(11)	138.13(9)
N(1)-Os(1)-C(3)	153.87(6)	120.74(13)	172.30(9)
N(1)-Os(1)-C(4)	160.55(6)	157.23(12)	139.24(8)
N(1)-Os(1)-C(5)	123.56(6)	157.24(10)	107.38(8)
N(1)-Os(1)-C(6)	97.02(6)	118.92(9)	92.69(8)
C(11)-Os(1)-Cl(1)	86.61(4)		
N(1)-Os(1)-Cl(1)	85.26(4)		
C(1)-Os(1)-Cl(1)	153.76(4)		
C(2)-Os(1)-Cl(1)	158.18(5)		
C(3)-Os(1)-Cl(1)	119.82(5)		
C(4)-Os(1)-Cl(1)	93.16(5)		
C(5)-Os(1)-Cl(1)	93.01(4)		
C(6)-Os(1)-Cl(1)	116.74(4)		
N(31)-Os(1)-C(1)		157.54(9)	
N(31)-Os(1)-C(2)		120.02(9)	
N(31)-Os(1)-C(3)		94.24(9)	
N(31)-Os(1)-C(4)		91.15(9)	
N(31)-Os(1)-C(5)		116.34(10)	
N(31)-Os(1)-C(6)		154.70(10)	
C(11)-Os(1)-N(31)		87.58(8)	
N(1)-Os(1)-N(31)		85.65(7)	
N(23)-Os(1)-C(1)			169.08(8)
N(23)-Os(1)-C(2)			136.31(9)
N(23)-Os(1)-C(3)			102.35(9)
N(23)-Os(1)-C(4)			88.16(8)
N(23)-Os(1)-C(5)			103.57(8)
N(23)-Os(1)-C(6)			136.90(8)
N(1)-Os(1)-N(23)			83.57(8)
C(11)-Os(1)-N(23)			86.21(8)

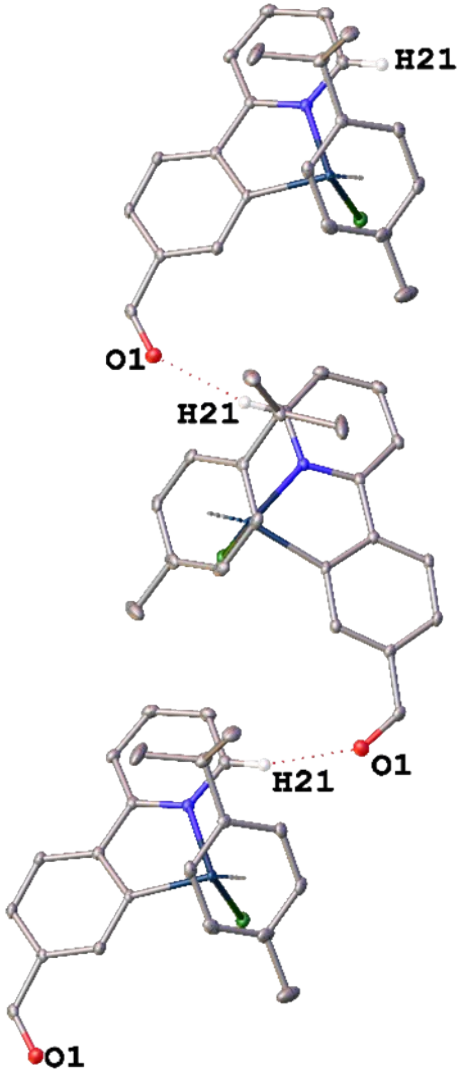

Figure S46. Schematic showing close contacts in complex **3a**.

Table S3. Close contacts for complex **3a** [Å and °].

D-H...A	d(D-H)	d(H...A)	d(D...A)	<(DHA)
C(21)-H(21)...O(1)#1	0.95	2.41	3.346(2)	166.8

Symmetry transformations used to generate equivalent atoms: #1 x+1/2,-y+3/2,z+1/2

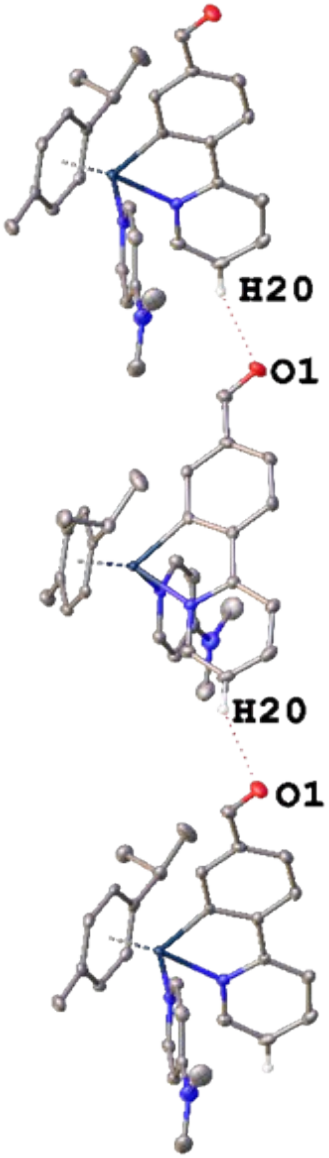

Figure S47. Schematic showing close contacts in complex **5a.**

Table S4. Close contacts for complex **5a** [Å and °].

D-H...A	d(D-H)	d(H...A)	d(D...A)	<(DHA)
C(20)-H(20)...O(1)#1	0.95	2.47	3.309(3)	147.9

Symmetry transformations used to generate equivalent atoms: #1 x+1/2,-y+3/2,z+1/2

10. Morphological analysis of A2780 cells

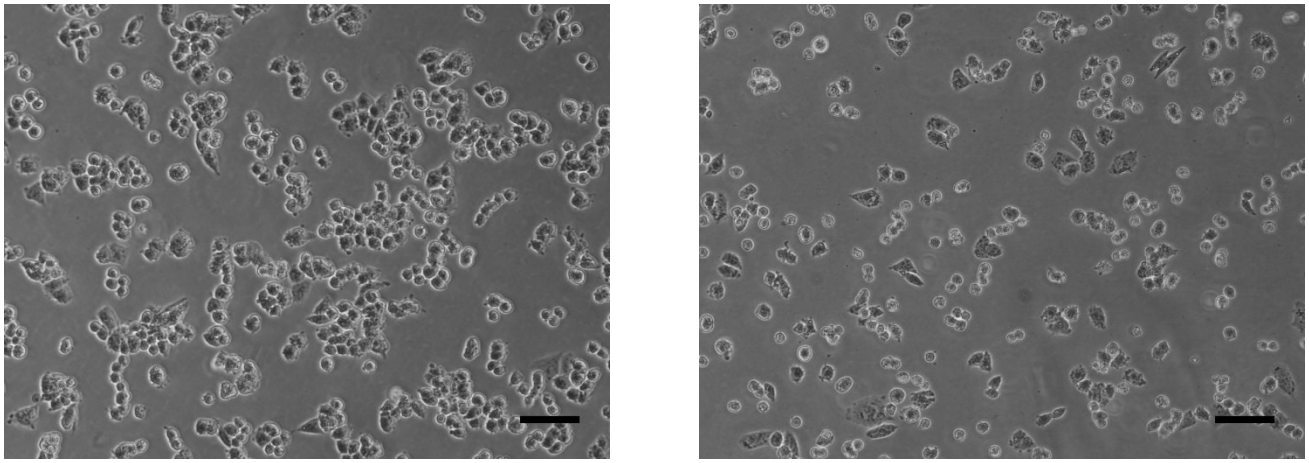

Untreated control

Complex **5a** (5 μM)

Figure S48. Cellular morphology of A2780 cells upon 24 h treatment with complex **5a** visualized under phase contrast NIKON Eclipse TE 2000U microscope. Scale bar = 100 μm.

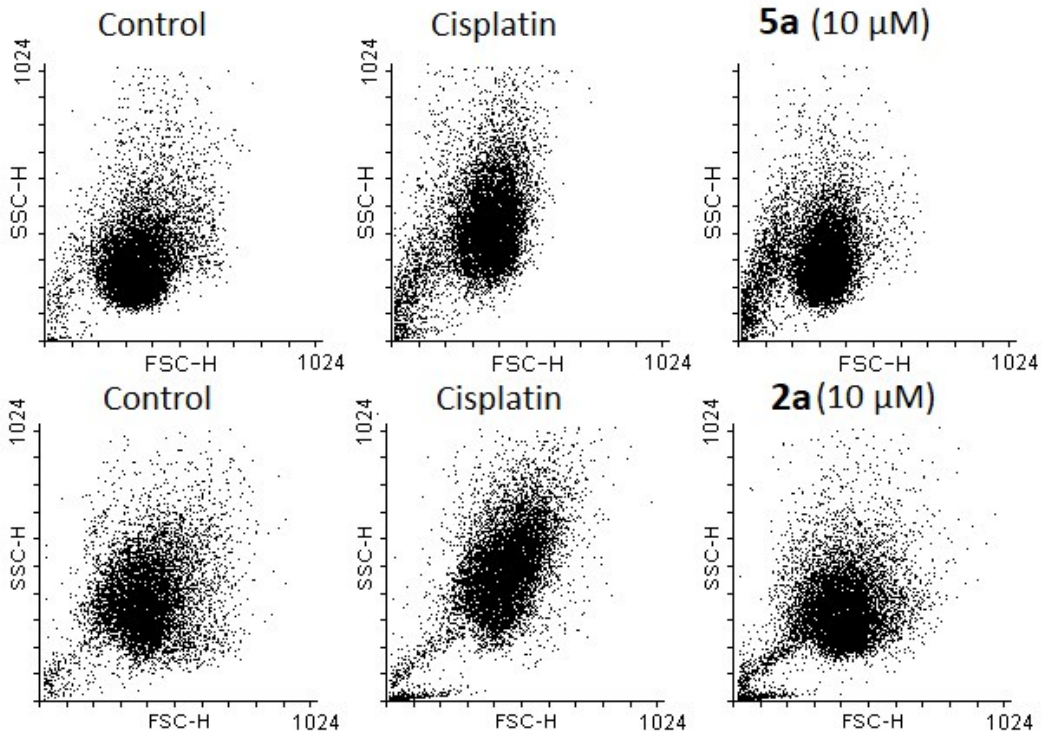

Figure S49. Effect of complexes **2a** and **5a** in the morphological analysis of A2780 evaluated by flow cytometry after 24 h treatment. Cisplatin (10 μM) was used as positive control. FSC-H: forward scatter, SSC-H: side scatter.

11. Measurement of the mitochondrial membrane potential.

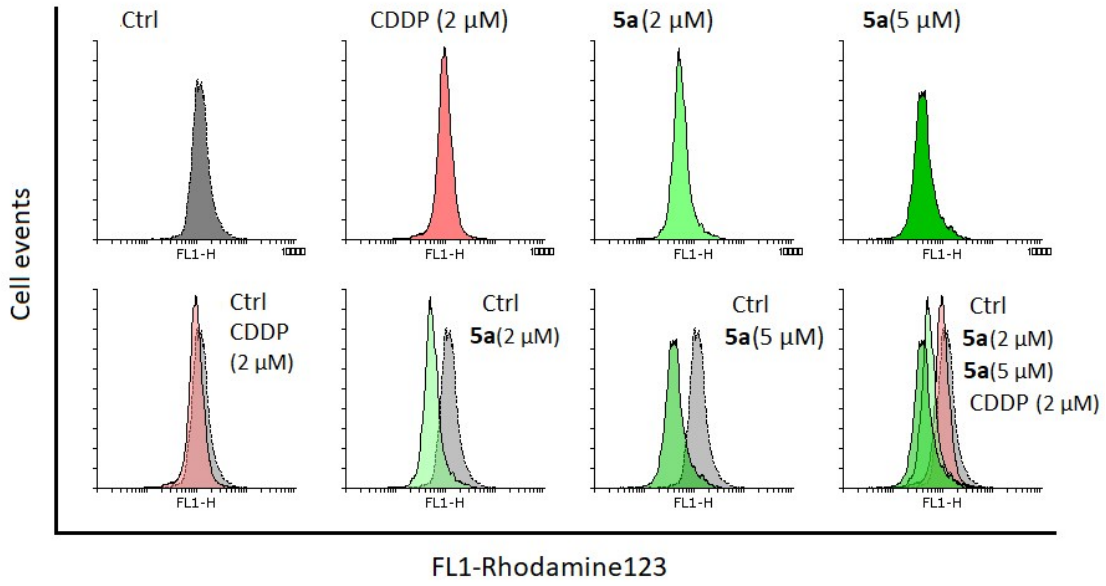

Figure S50. Impact on A2780 mitochondrial membrane potential evaluated by flow cytometry using Rhodamine123 dye in the FL1 channel after 24 h treatment with complex **5a** or cisplatin.

12. Cell death induction assays.

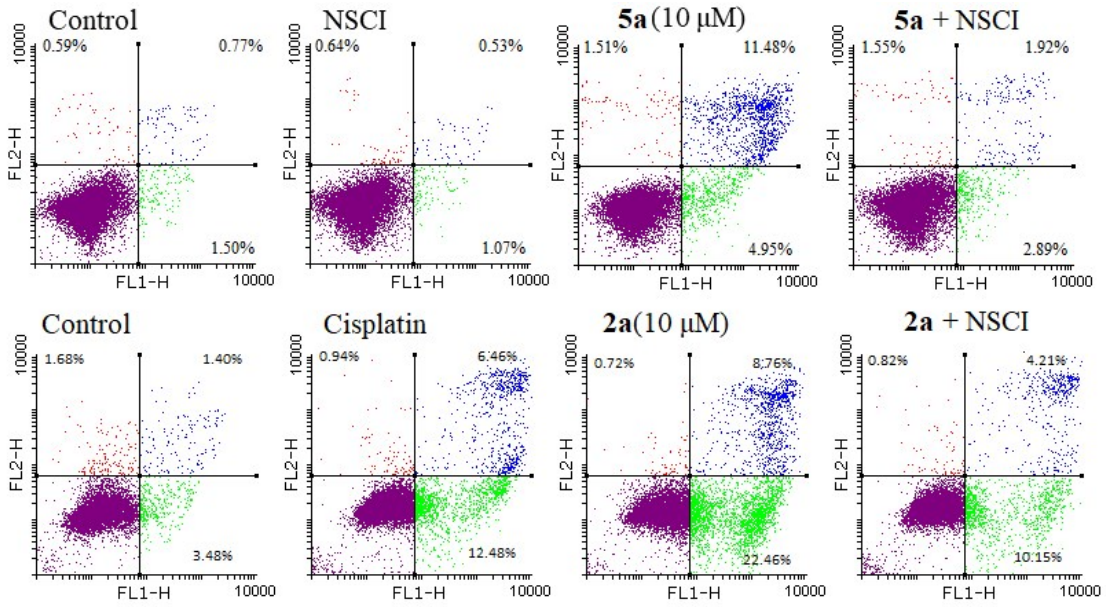

Figure S51. Representative flow cytometry dot plots of dual AnnexinV(FL1-H)/Propidium iodide (FL2-H) staining for apoptosis/necrosis induction evaluation. Cells were treated for 24h with **2a**, **5a** alone or subsequent to pretreatment with caspase 3 inhibitor NSCI (5 µM) for 1 h. Cisplatin (5 µM) was used as a positive control.

13. Cell cycle analysis.

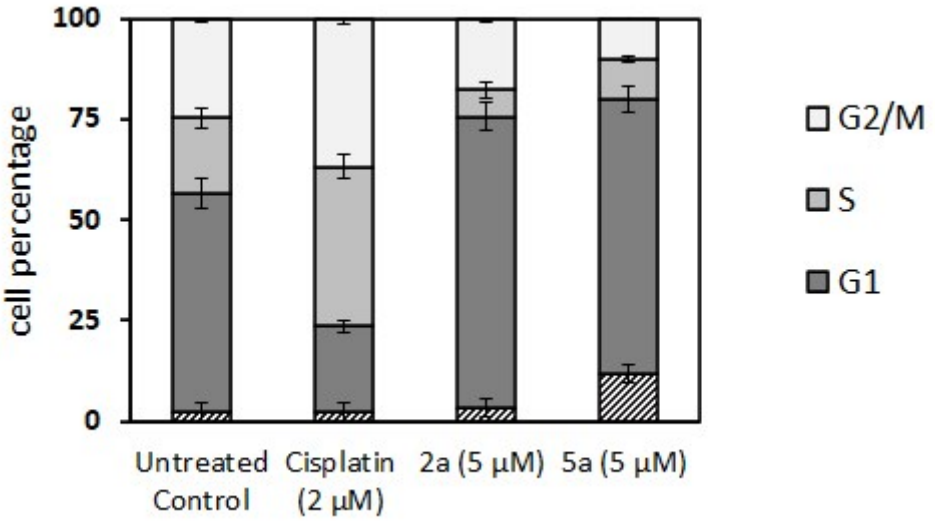

Figure S52. Cell cycle analysis of A2780 treated with either complex **2a, 5a** or cisplatin at indicated concentrations for 24 h measured using Propidium iodide intensity by flow cytometry in the FL2-A channel (n=2 replicates).

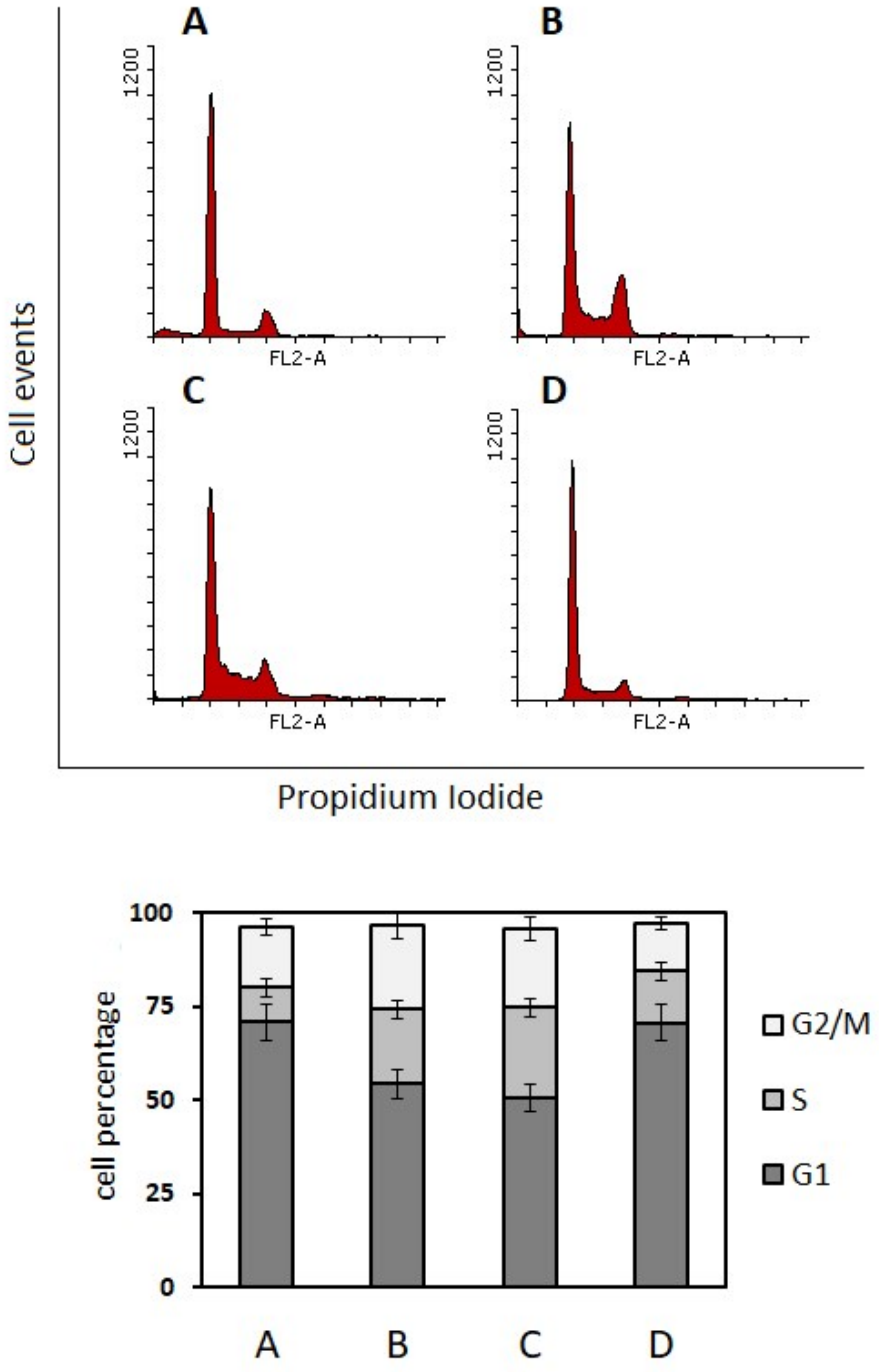

Figure S53. Cell cycle reversibility test in A2780 cells. Cells were synchronized by serum starvation to G1 phase during 24 h, treated with 2 μM **5a** for either 6 or 24 h. After drug exposure period, cells were returned to serum-containing cell media for another 24 h to re-enter cell cycle progression. A) G1-enriched cells by serum starvation, B) G1-released cells, C) 6 h **5a**-treated cells, D) 24 h **5a**-treated cells. Propidium iodide intensity was measured by flow cytometry in the FL2-A channel.

14. Protein synthesis inhibition assay

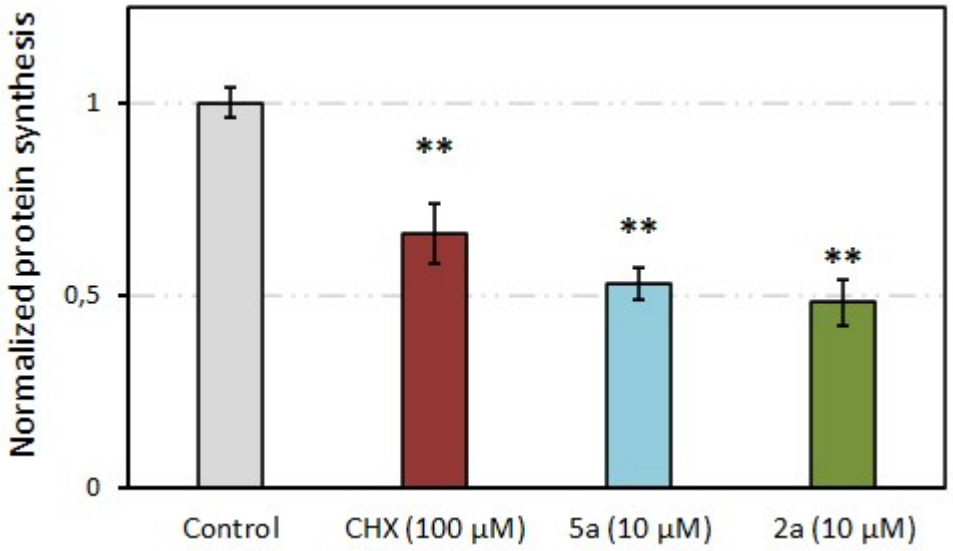

Figure S54. Normalized translation levels measured by O-propargyl-puromycin incorporation in nascent proteins using Click-iT Alexa Fluor-OPP Kit (Thermofisher) after treatment for 12 h with either **2a, 5a** or cycloheximide (CHX), which was used as a positive control. Data are representative of two independent experiments and represented as mean ± SD **p<0.01 (student t-test).

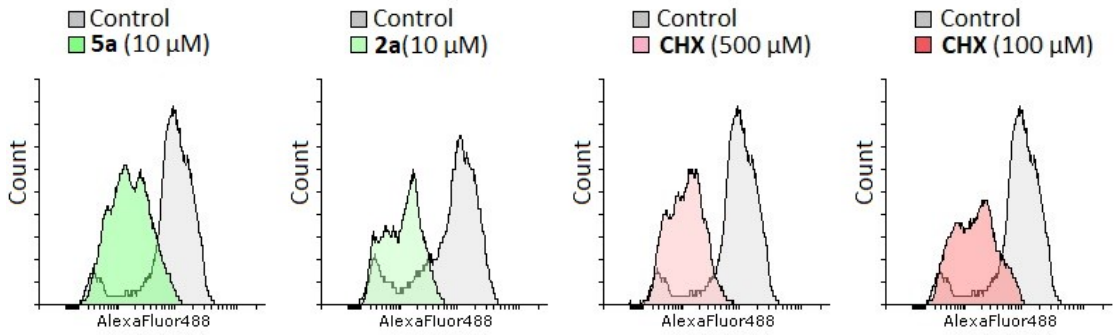

Figure S55. Flow cytometry analysis of O-propargyl-puromycin incorporation in nascent proteins using Click-iT Alexa Fluor-OPP Kit (Thermofisher). Fluorescence of AlexaFluor488 was measured in FL1-H channel after treatment for 12 h with either complex **2a, 5a** or cycloheximide (CHX) as a positive control. Data are representative of two independent experiments.

15. ROS generation

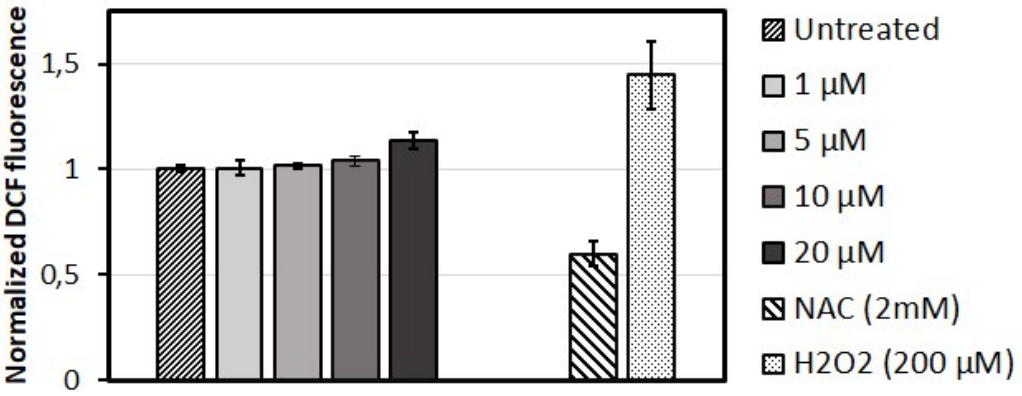

Figure S56. ROS levels in A2780 after 2 h exposure of complex **5a** at indicated concentrations measured using DCFH-DA probe. Untreated cells were used as a negative control, N-acetyl-cysteine (NAC) was used as a positive control for ROS scavenging and hydrogen peroxide (H_2O_2), as a positive control for ROS generation.

16. Tumor size evaluation

The obtained bright-field images were used to measure the area of each tumorous gonad by using the ImageJ software [1]. Gonad sizes were measured from the loop region to the proximal region, including uterus area when it was filled with tumorous cells. Significance of the obtained data was performed by the ANOVA test with a significance level of 0.5.

Figure S57. Effect on tumor growth of complex **5b**. Representative images taken at 20x of: (A) 0.1 % DMSO (control) treated animal, (B) 100 μM complex **5b** in 0.1 % DMSO, in all the cases the tumor is outlined in blue. Scale bar: 100 μm.

Table S5: Tumor size data.

	C (µM)	n	Gonad Size (µm²)	S. D	Change (%)	*p* value *vs* control
CDDP	0	39	14504.92	3184.982	0.00	
	0.1	16	13129.62	1611.226	-9.48	0.107553
	1	16	13265.06	1891.873	-8.55	0.152728
	10	36	10435.45	2128.697	-28.06	<0.00001
	100	47	7408.581	2149.854	-48.92	<0.00001
Complex 5a	0	12	13339.67	1618.312	0.00	
	0.1	20	12976.09	2532.537	-2.73	0.660005
	1	18	12949.04	2137.884	-2.93	0.613771
	10	18	11093.36	1323.740	-16.84	0.000896
	100	34	10773.92	1901.112	-19.23	0.000143
Complex 5b	0	39	14581.19	1957.911	0.00	
	0.1	20	14687.63	1737.061	0.73	0.840867
	1	20	14606.76	1373.826	0.18	0.960106
	10	21	12989.33	1836.192	-10.92	0.00378
	100	53	10119.56	2554.976	-30.60	<0.00001
Complex 2a	0	73	16552.92	2856.43	0.00	
	0.1	58	14139.82	2379.38	-14.58	<0.00001
	1	59	11217.88	2101.39	-32.23	<0.00001
	10	57	13493.89	2232.82	-18.48	<0.00001
	100	74	13445.74	2342.75	-18.77	<0.00001

17. Survival assays

Table S6: Lifespan assays survival data.

		C (µM)	n	days	S. E	Change in Lifespan (%)	*p* value vs control
JK1466 (*gld-1*)	**CDDP**	0	74	8.32	0.2	0.00	
		0.1	42	8.7	0.23	4.57	0.5218
		1	60	8.42	0.21	1.20	0.9642
		10	53	9.77	0.21	**17.43**	0.0001
		100	46	9.82	0.17	**18.03**	0.0008
	Complex 5a	0	46	8.33	0.25	0.00	
		0.1	44	8.15	0.28	-2.16	0.9029
		1	44	9.4	0.24	**12.85**	0.0328
		10	31	9.74	0.32	**16.93**	0.0005
		100	40	8.87	0.5	6.48	0.019
	Complex 5b	0	115	8.46	0.18	0.00	
		0.1	96	8.68	0.2	2.60	0.2929
		1	100	8.95	0.18	**5.79**	0.0429
		10	127	9.12	0.14	**7.80**	0.0403
		100	101	9.45	0.14	**11.70**	0.0002
	Complex 2a	0	184	8.6	0.18	0.00	
		0.1	168	8.63	0.15	0.35	0.4436
		1	116	9.14	0.2	**6.28**	0.0327
		10	124	9.31	0.19	**8.26**	0.0001
		100	92	9.31	0.31	**8.26**	0.0512
N2 (Wild-type)	**CDDP**	0	136	10.76	0.1	0.00	
		0.1	52	10.65	0.11	-1.02	0.2366
		1	133	10.28	0.09	-4.46	0.002
		10	98	12.5	0.17	**16.17**	0
		100	81	12.04	0.15	**11.90**	0
	Complex 5a	0	167	9.65	0.06	0.00	
		0.1	134	9.08	0.11	-5.91	0.0008
		1	151	10.04	0.1	4.04	0.0001
		10	66	11.17	0.18	**15.75**	0
		100	55	11.24	0.24	**16.48**	0
	Complex 5b	0	192	10.82	0.27	0.00	
		0.1	178	11.09	0.31	2.50	0.8308
		1	140	11.25	0.22	3.97	0.2302
		10	114	11.3	0.22	**4.44**	0.0261
		100	188	11.23	0.25	3.79	0.7807
	Complex 2a	0	128	11.05	0.11	0.00	
		0.1	72	12.1	0.13	9.50	0.000003

		1	118	12.54	0.17	**13.48**	0.0000001
		10	72	10.5	0.12	-4.98	0.003
		100	133	10.28	0.09	-6.97	0.0000037

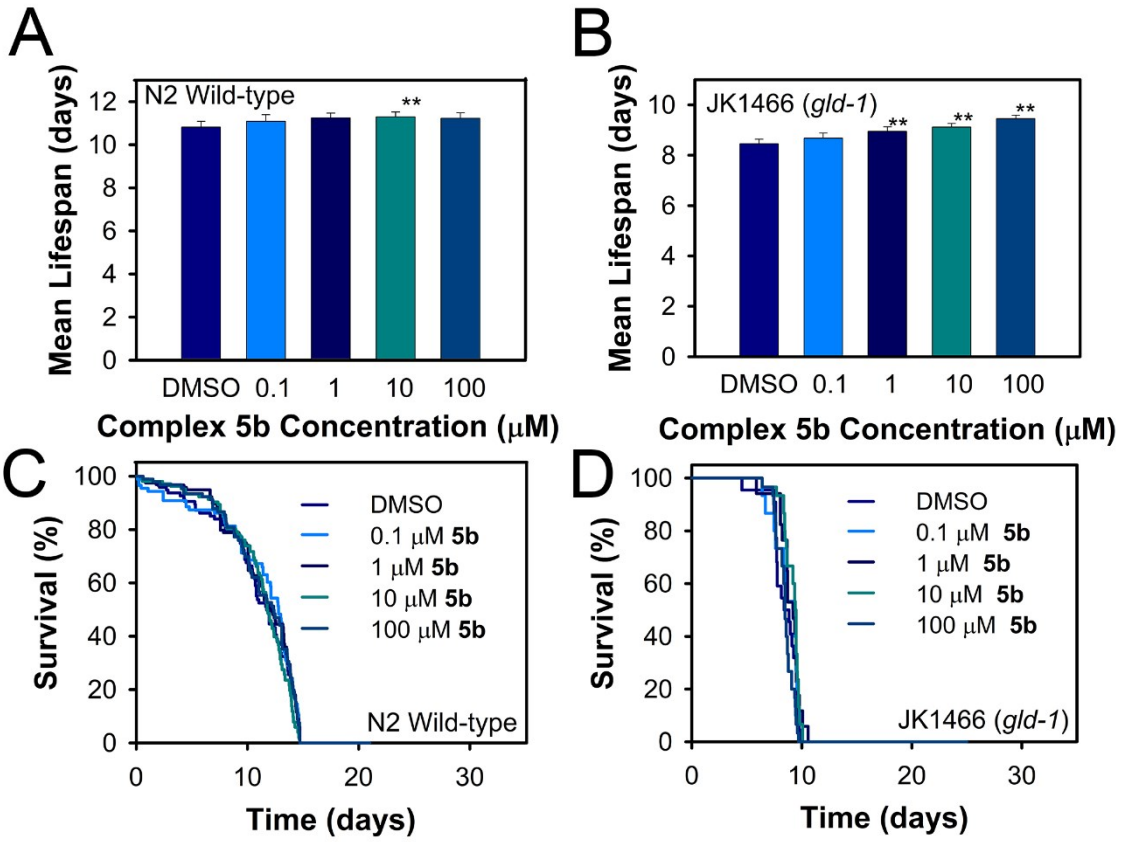

Figure S58. Toxicity effect of complex **5b.** Lifespan histograms and survival curves for the strains N2 and JK1466 treated with different concentrations of **5b**. Data is presented as mean ± SE, ** significative at $p \leq 0.05$

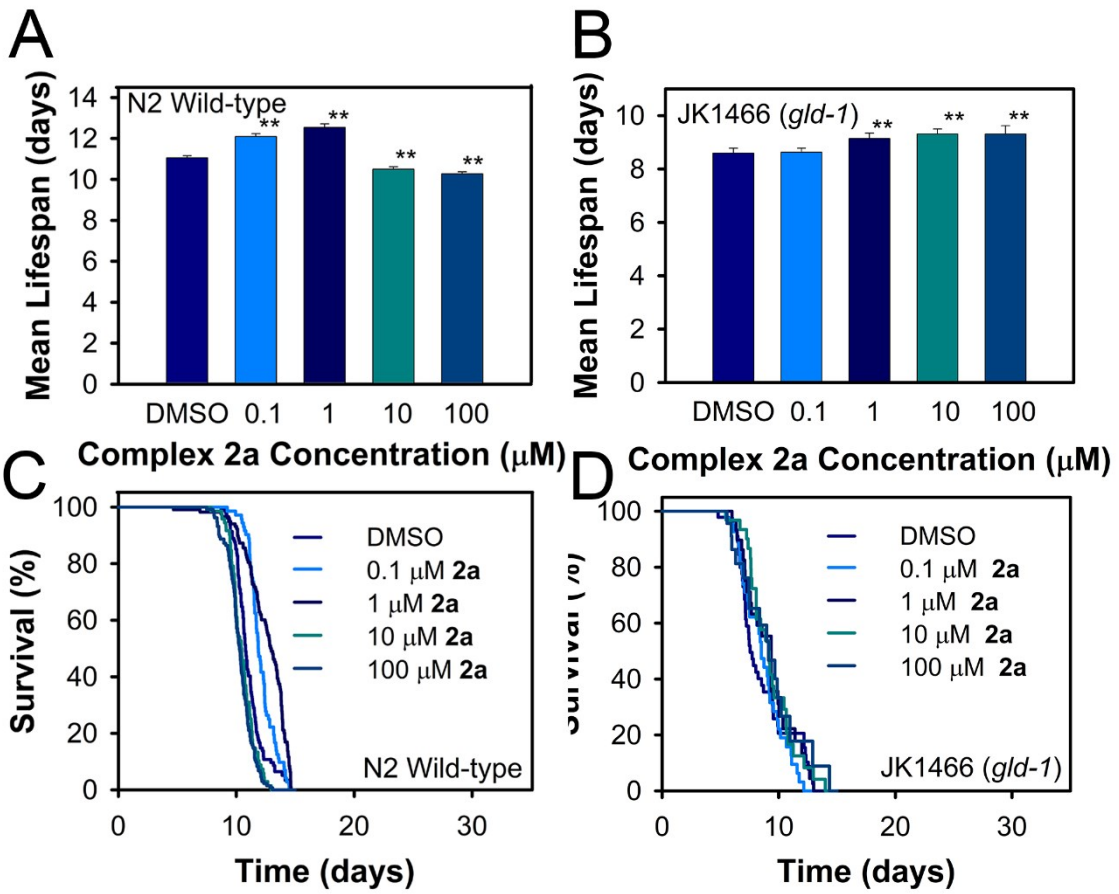

Figure S59. Toxicity effect of complex **2a.** Lifespan histograms and survival curves for the strains N2 and JK1466 treated with different concentrations of **2a**. Data is presented as mean ± SE, ** significative at $p \leq 0.05$

18. Effect of the metallic complexes in ROS production *in vivo*

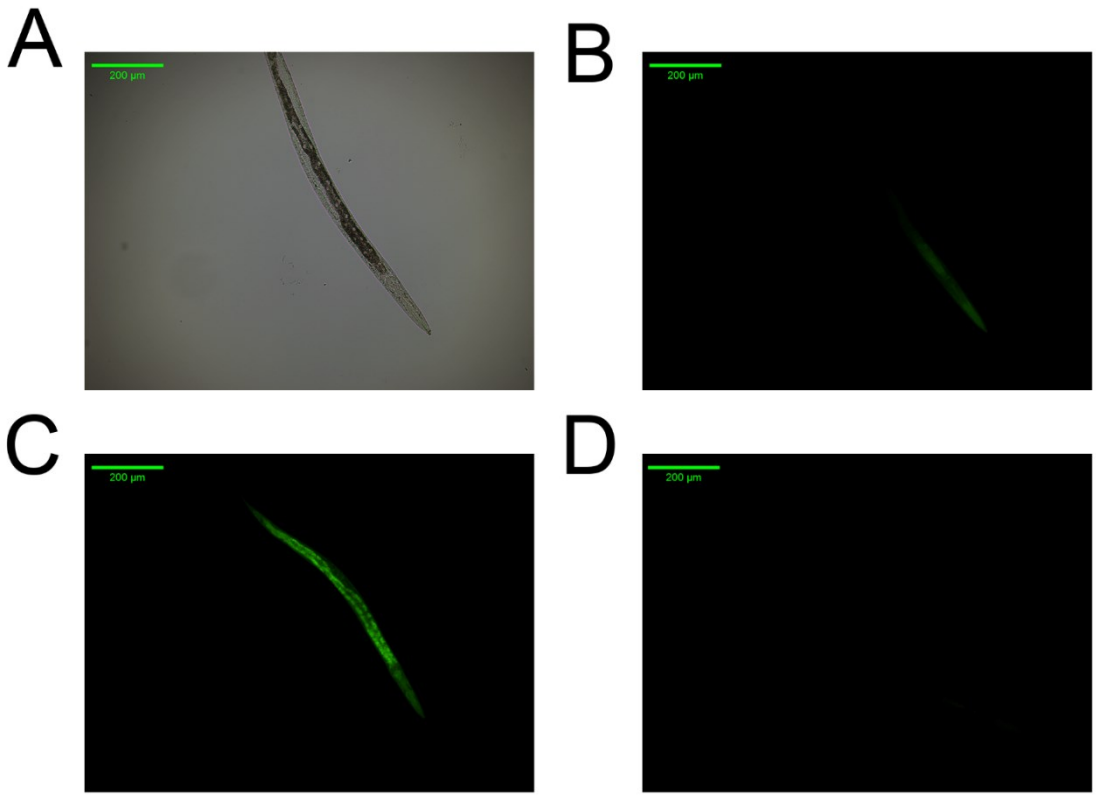

Figure S60. Effect of the metal complexes in ROS production. Representative images of: (A) *C. elegans* wild-type bright-field, (B) Positive control (treated with juglone), (C) Animals treated with 100 µM CDDP, (D) Worms treated with 100 µM **5a**. scale bar: 200 µm.

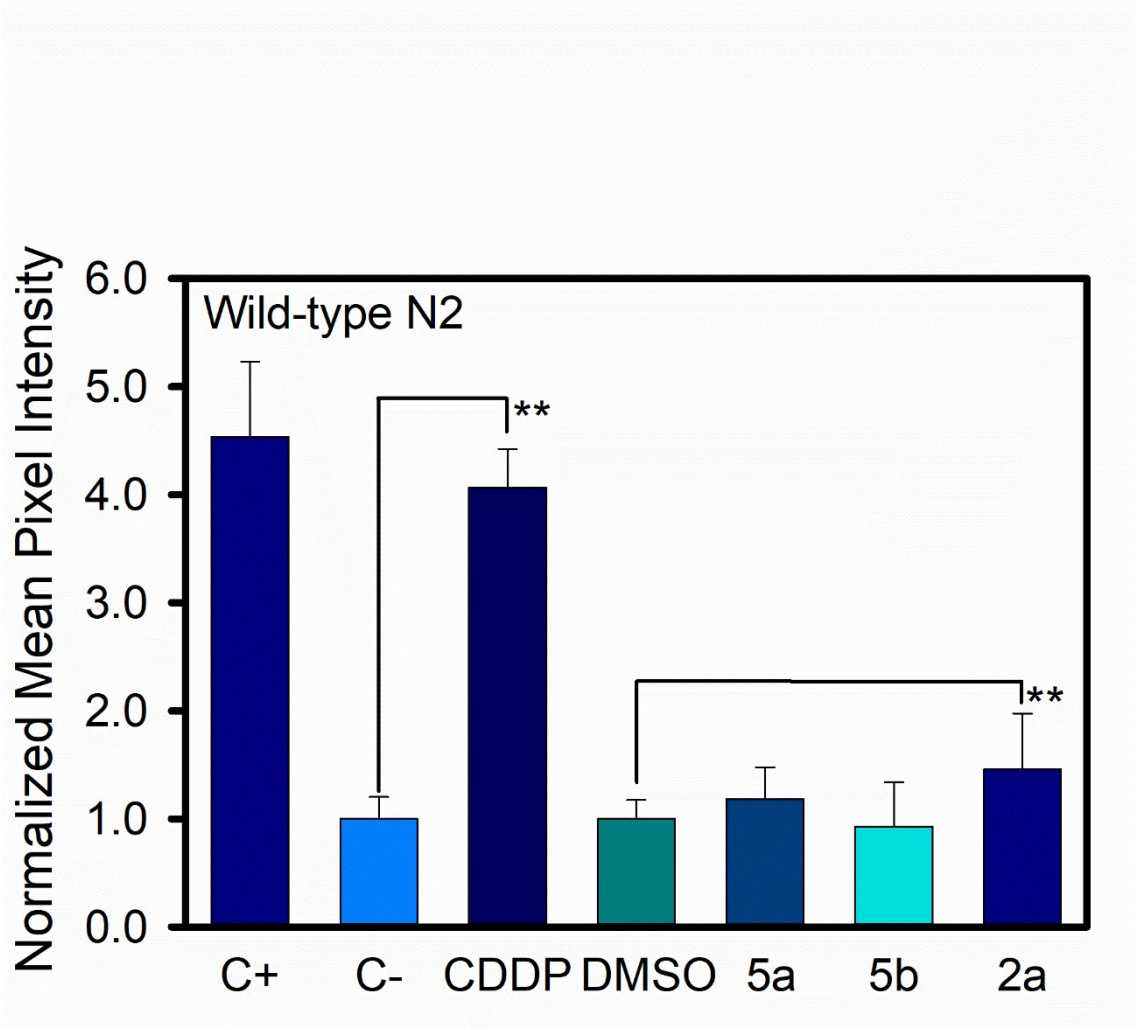

Figure S61. Metallic complexes effect in ROS production *in vivo*. Integrated fluorescence of the *C. elegans* wild-type, treated with the metal complexes (100 μM) or juglone (20 μM) and stained with DCFH-DA (MEAN ± SEM), n ≥10, two independents trials were measured in each case, ** $p \leq 0.05$ by ANOVA test.

19. Effect of 4a, 4b and CDDP on HSP-16.2p expression

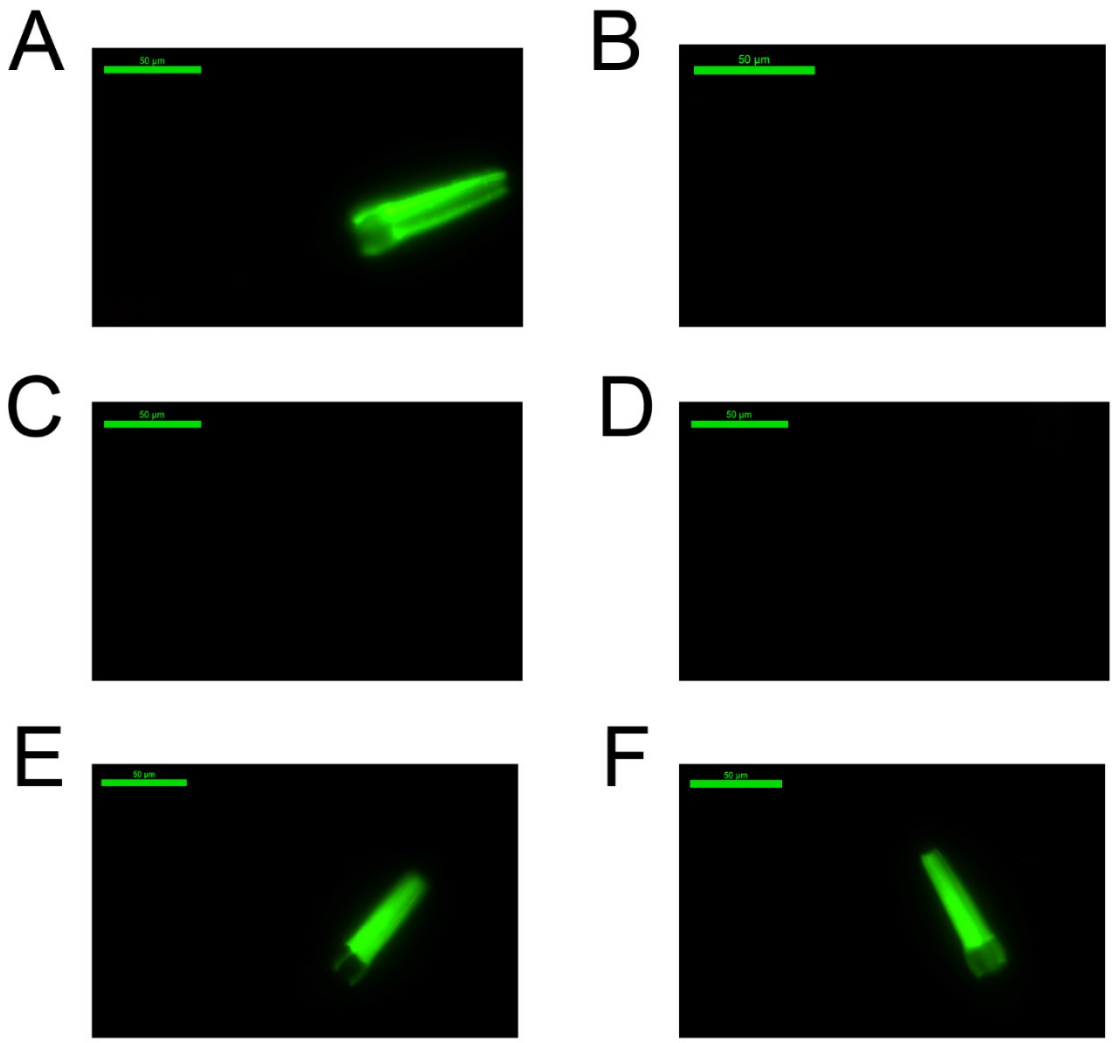

Figure S62. Effect of the metal complexes in oxidative stress resistance. Representative images of: (A) Positive control (treated with juglone), (B) Control negative, (C) Animals treated with 100 µM CDDP, (D) Worms treated with 100 µM complex **5a**, (E) Animals treated with 100 µM CDDP (48 h) and 20 µM juglone (24 h) and (F) Animals treated with 100 µM complex **5a** (48 h) and 20 µM juglone (24 h). scale bar: 50 µm.

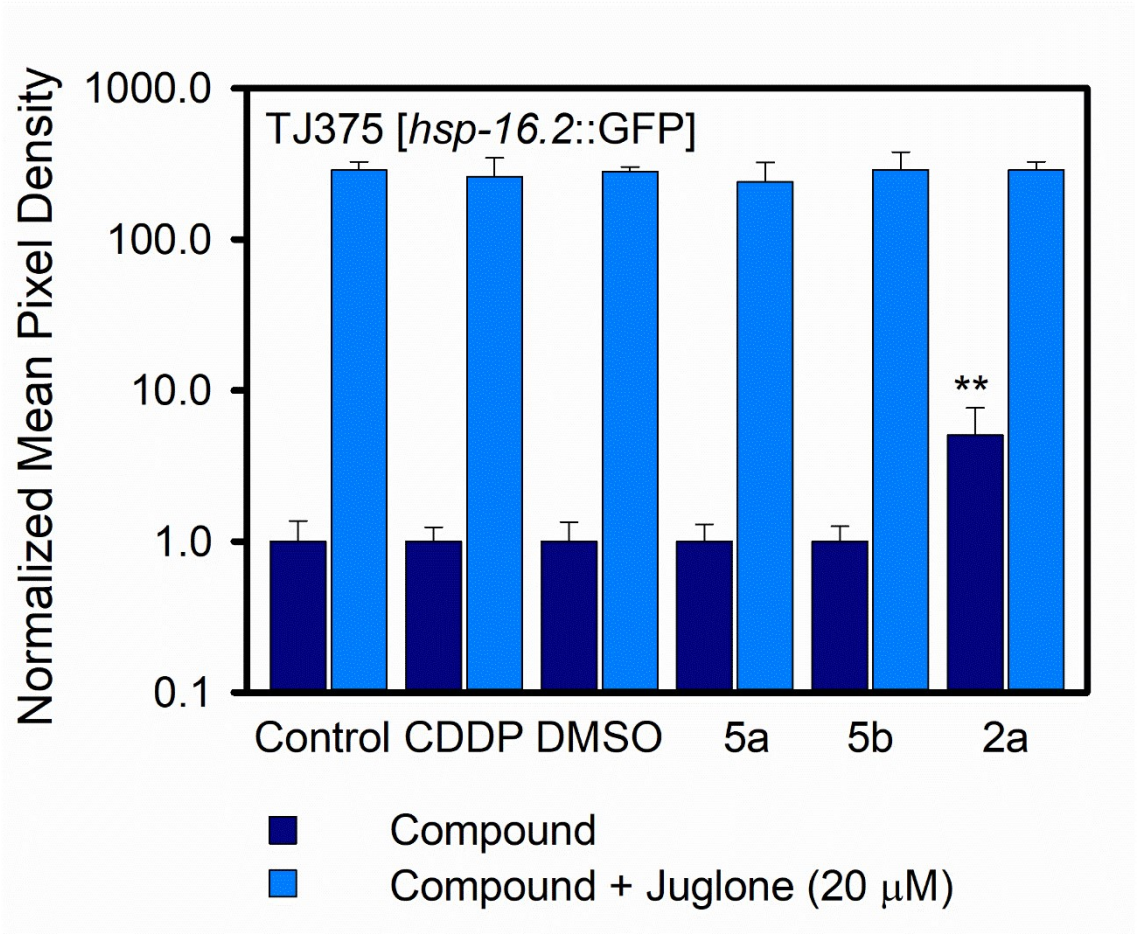

Figure S63. Effect of the metal complexes in HSP-16.2::GFP expression. Integrated fluorescence of the TJ375 *C. elegans* strain, treated with the metal complexes (100 μM) with or without juglone (20 μM) (MEAN ± SEM), n ≥10, two independents trials were measured in each case, the results were not significative by ANOVA test.

20. Effect of 5a, 5b and CDDP on SOD-3 expression

Synchronous cohorts of the CF1553 strain were treated with 100 μM of each drug or their vehicle for 48 hours at 20 ºC in S medium, juglone 20 μM was used as positive control. Then worms were washed with M9 and visualized under fluorescence microscope at 20x lens with the I3 filter cube. The image acquisition and analysis were performed as above. Whereas the SOD-3 is accumulated in the head, the tail and the vulva of the animals, only the head fluorescence was used to measure the SOD-3 accumulation.

21. Effect of 4a, 4b and CDDP on GST-4p expression

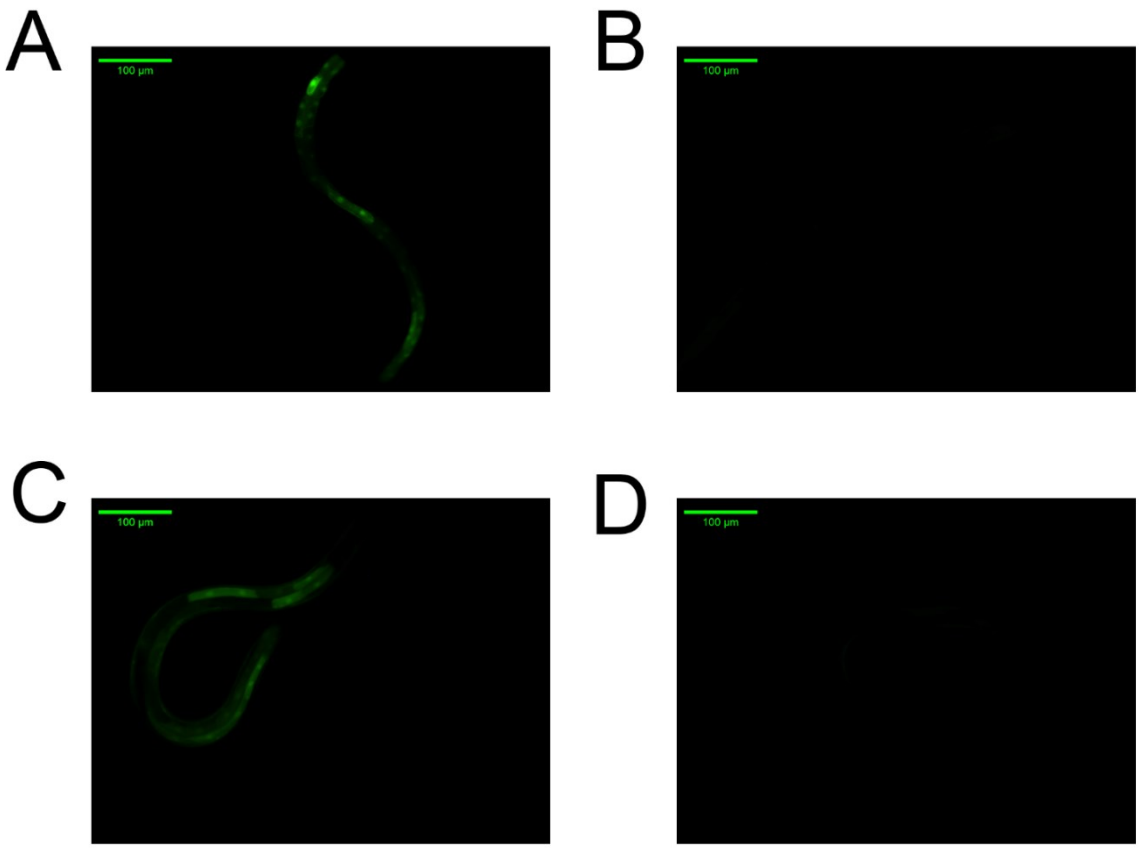

Figure S64. Effect of the metal complexes in GST-4 expression. Representative images of: (A) Positive control (CL2166 strain treated with juglone), (B) Control negative, (C) Animals treated with 100 µM CDDP, (D) Worms treated with 100 µM complex **5a**. Scale bar: 100 µm.

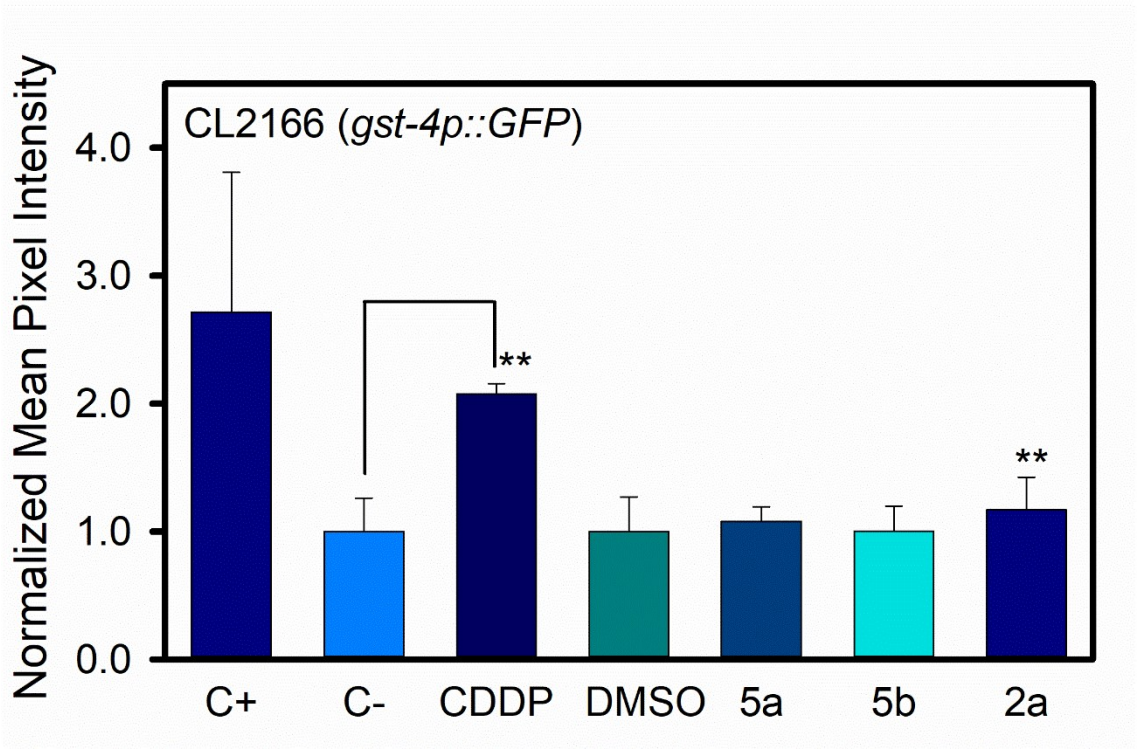

Figure S65. Effect of the metal complexes in GST-4::GFP expression. Integrated fluorescence of the CL2166 *C. elegans* strain, treated with the metal complexes (100 μM) or with juglone (20 μM) (MEAN ± SEM), n ≥10, two independents trials were measured in each case, ** significative at $p \leq 0.05$ by ANOVA test.

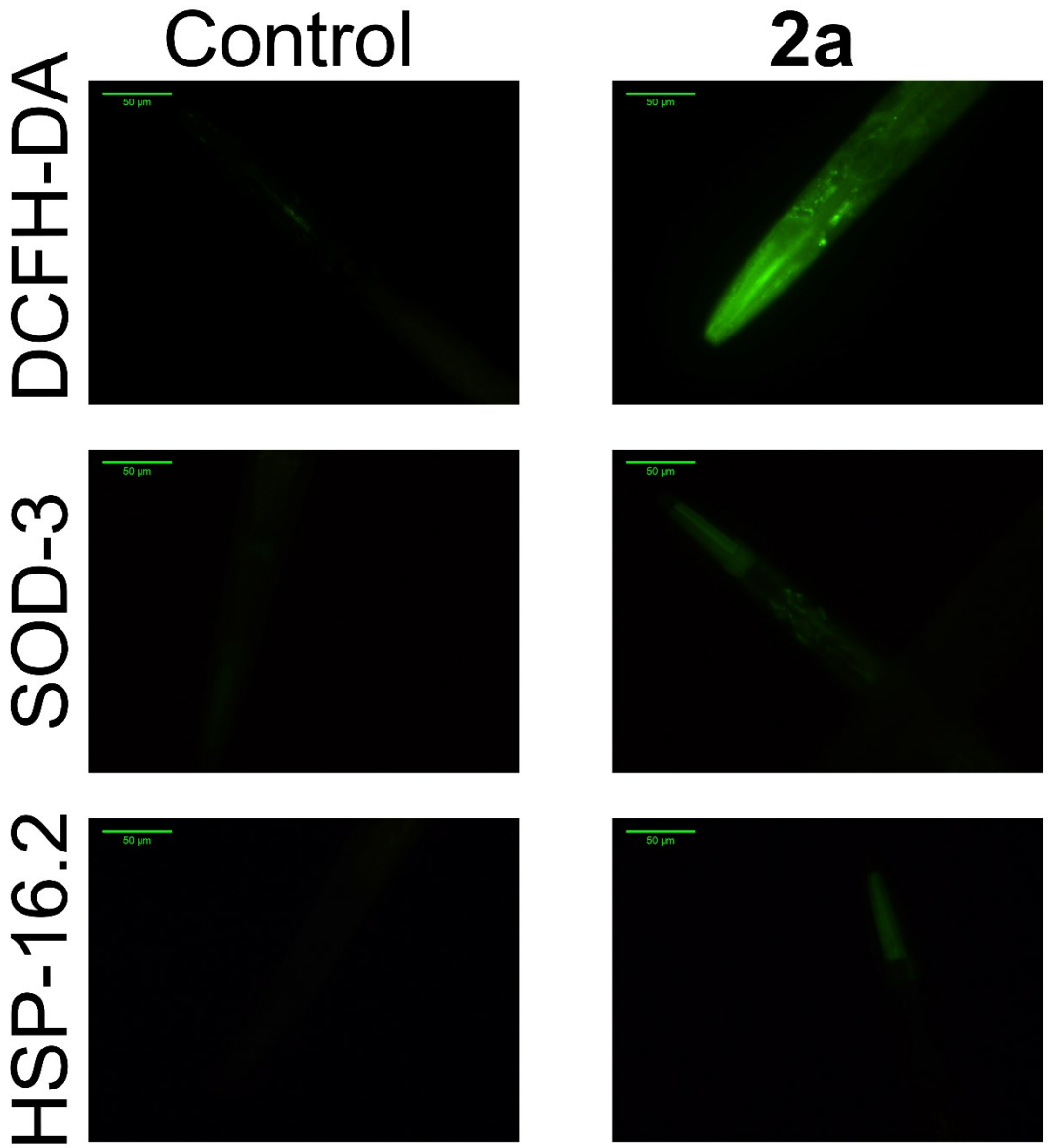

Figure S66. Effect of the complex **2a** on ROS production, SOD-3 and HSP-16.2 expression. Representative images of N2 stained with DCFH-DA, CF1553 strain and TJ375 strain treated either with DMSO (control) or with 100 µM of complex **2a**. Scale bar: 50 µm.

22. References

1 C. A. Schneider, W. S. Rasband and K. W. Eliceiri, *Nature Methods*, 2012, **9**, 671–675.